

I give permission for public access to my Honors paper and for any copying or digitization to be done at the discretion of the College Archivist and/or the College Librarian.

Signed

Megan Elizabeth Hotard

[Megan Elizabeth Hotard]

Date

April 22, 2014

Bio-guided Natural Product Drug Discovery Platform Focused on All-Carbon
Spirocenter Containing Molecules

Megan Elizabeth Hotard

Department of Chemistry

Rhodes College

Memphis, TN

Rivas Laboratory

Department of Chemical Biology and Therapeutics

St. Jude Children's Research Hospital

Memphis, TN

2014

Submitted in partial fulfillment of the requirements for the Bachelor of Science
degree with Honors in Chemistry

This Honors paper by Megan Hotard has been read
and approved for Honors in Chemistry.

Dr. Fatima Rivas

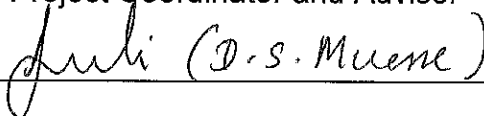
Extra-Departmental Reader

St. Jude Project Advisor



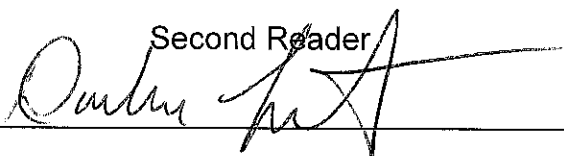
Dr. Dhammika Muesse

Project Coordinator and Advisor



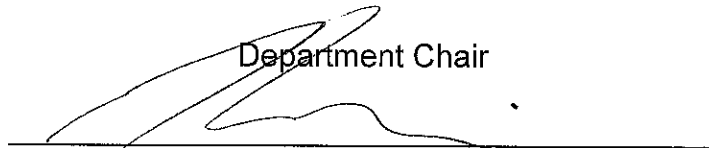
Dr. Darlene Loprete

Second Reader



Dr. Mauricio Cafiero

Department Chair



Acknowledgements

First, I would like to acknowledge the St. Jude Summer Plus Program for granting me the initial opportunity to work in the Rivas laboratory as part of their fellowship program. I would like to acknowledge my mentor and St. Jude faculty sponsor, Dr. Fatima Rivas, for her patience and guidance over the past two years, specifically throughout the course of this project. I would like to thank all of my Rivas lab members, especially Dr. Taatao Ling for his training and assistance in lab, and Dr. Adaris Rodrigues-Cortes for further explanations on the biological applications of this project and conducting all of the wound healing assays. I would also like to acknowledge the Rhodes College Chemistry Department and their support in helping me continue my research at St. Jude by accepting my petition for honors research. Additionally, the flexibility and support of my thesis committee members Dr. Dhammika Muesse and Dr. Darlene Loprete enabled me to successfully complete this off campus project. Finally, I would like to acknowledge ALSAC for funding this project.

Table of Contents

Signature page.....	i
Acknowledgements.....	ii
Table of Contents.....	iii
List of Tables, Figures, and Schemes.....	iv
Abstract.....	v
Abbreviations.....	vi
Introduction.....	1
Natural Products.....	1
Ene Reaction Approach to All-Carbon Spirocenters.....	6
Therapeutic Focus: Wound Healing.....	10
Objectives.....	14
Discussion and Results.....	17
Extraction, Isolation, and Structure Elucidation of Pteropodine.....	17
Structure-Activity Relationship Evaluation of Pteropodine.....	19
Ene Reaction Model Study A: All-Carbon Spirocyclic Compounds.....	19
Ene Reaction Model Study B: Indole Spirocyclic Compounds.....	21
Biological Studies via Cicatrisation Assays.....	25
Conclusions.....	31
Supporting Information.....	32
References.....	52

List of Figures

Table 1: Natural Product Drug Discovery Platform.....	2
Table 2: Results of Screening Conditions for Model B Compounds.....	25
Table 3: List of Compounds Tested via Migration Assay.....	27
Table 4: List of Controls for Migration Assay.....	28
Figure 1: Bio-Guided Natural Product Drug Screening Platform.....	3
Figure 2: <i>Uncaria Tomentosa</i> Natural Products Summary.....	4
Figure 3: <i>Uncaria Tomentosa</i> Natural Products featuring Spirocyclces	5
Figure 4: Proposed Ene Reaction Mechanism.....	7
Figure 5: Advances on the Ene Reaction.....	9
Figure 6: Role of Macrophages in Wound Healing.....	12
Figure 7: Proposed All-Carbon Spirocyclization Reaction (Model A).....	15
Figure 8: Proposed Indole Spirocyclization Reactions (Model B).....	16
Figure 9: Compounds Isolated from <i>Uncaria tomentosa</i>	18
Figure 10: 2D characterization of pteropodine using COSY.....	18
Figure 11: Gap-Closure Migration Assay.....	26
Figure 12: Migration Assay Results.....	29
Scheme 1: Structure-Activity Relationship Evaluation of Pteropodine.....	19
Scheme 2: Synthesis of Key Intermediate 9 and Promising Lead Reaction Conditions for All-Carbon Spirocyclces.....	20
Scheme 3: Synthesis of Precursor 18	22

Abstract

Bio-guided Natural Product Drug Discovery Platform Focused on All-Carbon Spirocenter Containing Molecules

Megan Elizabeth Hotard

Natural products remain a vibrant source of novel compounds that can serve as molecular probes or therapeutic agents. Of specific interest among biologically active terrestrial natural products are spirocycles, which are characterized by either a tertiary or quaternary carbon spirocenter. Intrigued by the potential of these natural products as potential wound healing agents, we began a campaign to isolate, characterize, and develop methodologies towards such spirocycle molecules. Herein, we disclose our findings featuring the natural product pteropodine, a pentacyclic oxindole with a spirocenter, as the inspiration to develop spirocycle methodologies. We have successfully isolated pteropodine from the plant *Uncaria tomentosa* and utilized this natural product as a potential lead. We also developed new methodologies to access these spirocycles after hypothesizing that a metal-mediated ene-type reaction could proceed under mild reaction conditions and tolerate a broad range of substituents to provide functionalized structures. The chemical reactions were carried out under inert atmosphere, monitored by thin layer chromatography, and analyzed by Mass Spectrometry and Nuclear Magnetic Resonance. The biological properties of these compounds in a gap closure migration assay are presented.

Abbreviations

2D NMR	Two Dimensional Nuclear Magnetic Resonance
ADA	American Diabetes Association
AgOTf	Silver trifluoromethanesulfonate
Boc	Di-tert-butyl dicarbonate
BuLi	Butyllithium
DCE	Dichloroethane
DIBAL-H	Diisobutylaluminum Hydride
DMSO	Dimethyl Sulfoxide
Et ₂ O	Diethyl Ether
HMPA	Hexamethylphosphoramide
HPLC	High Performance Liquid Chromatography
H ₂ SO ₄	Sulfuric Acid
I ₂	Iodine
KHMDS	Potassium bis(trimethylsilyl) amide
LDA	Lithium Diisopropylamide
Pd ₂ (dba) ₃	Tris(dibenzylideneacetone)dipalladium(0)
PPh ₃	Triphenylphosphine
MCL7	Breast cancer cell line
MDA-MB 231	Aggressive breast cancer cell line
MeOH	Methanol
NaClO	Sodium Hypochlorite
NP	Natural Products
ROS	Reactive Oxygen Species
SAR	Structure-Activity Relationship
STO	Mouse embryonic fibroblast cell line
TBAF	Tetrabutylammonium Fluoride
TMS	Tetramethylsilane
TMSCl	Trimethylsilyl chloride

Bio-guided Natural Product Drug Discovery Platform Focused on All-Carbon Spirocenter Containing Molecules

Introduction

Natural Products

Natural products offer a broad range of complex structures that have been used to inspire a variety of therapeutic agents to treat many illnesses ranging from cancer to infectious diseases. We chose to utilize the unique structures of these natural products as a source of inspiration for new therapeutic to accelerate the wound healing process. Considering that terrestrial natural products have been used for centuries to treat human disease, we pursued a bio-guided screening approach of natural products in pursuit of new potential therapeutic agents. This method of drug discovery has been utilized to contribute to 70% of antitumor agents approved by the FDA [1]. In order to carry out a thorough study, we focused on plants that are known to have been used by Native Americas for their medicinal purposes. We evaluated a focused library of plants from North and South America to be screened for activity against childhood malignancies and wound healing. As outlined in Table 1, North American plants studied included *Hydrastis Canadensis*, *Quercus dumosa*, *Aristolochia leuconeura*, *Phacelia hastate*, *Acer rubrum*, *Oenanthe sarmentosa*, and *Salvia mellifera*. Plants evaluated from South America include *Terminalia catappa*, *Uncaria tomentosa*,

Onoclea sensibilis, *Ligusticum cf. grayi*, *Dioscorea bulbifera*, *Cuphea hyssopifolia*, and *Solanum sisymbriifolium*. These plants were prime candidates for our natural product drug discovery platform due to their documented therapeutic effects as well as their prevalent use in traditional medicines by Native American healers.

North American Plants		South American Plants	
No.	Plant	No.	Plant
1	<i>Hydrastis canadensis</i>	1	<i>Terminalia catappa</i>
2	<i>Quercus dumosa</i>	2	<i>Uncaria tomentosa</i>
3	<i>Aristolochia leuconeura</i>	3	<i>Onoclea sensibilis</i>
4	<i>Phacelia hastata</i>	4	<i>Ligusticum cf. grayi</i>
5	<i>Acer rubrum</i>	5	<i>Dioscorea bulbifera</i>
6	<i>Oenanthe sarmentosa</i>	6	<i>Cuphea hyssopifolia</i>
7	<i>Solanum sisymbriifolium</i>	7	<i>Salvia mellifera</i>

Table 1: Natural Product Drug Discovery Platform

As illustrated in Figure 1, the bio-guided natural product drug screening platform commenced with the extraction of the stems and leaves of raw plant materials. The plant materials were minced and extracted with isopropanol under reflux conditions for two days as depicted in step 1. The isopropanol solution was filtered, and the remaining plant material was re-extracted for an additional two days. After decanting the solution from the remaining plant material, the two solutions were combined and concentrated in the second step. These crude extracts were pre-fractionated using a 20 g SNAP Biotage cartridge. Column conditions increased linearly from 0 to 100% ethyl acetate in hexane followed by

0 to 20 % methanol in ethyl acetate. Using this method, six fractions were produced for each of the fourteen natural products. Pending the results of biological studies, fractions that demonstrated activity were further purified using a 10 g SNAP Biotage cartridge, illustrated by step 4. Fractions were submitted for biological testing against several different catastrophic childhood malignancies including *plasmodium falciparum* as well as for their potential as wound healing therapeutics. Fractions were submitted for testing as 3 mg/mL solutions in DMSO for a target concentration of 10 mM (assuming a molecular weight of 300 g/mol). DNA stain-based assays were used to evaluate the fractions' potential against parasitic childhood malignancies, specifically malaria. To evaluate the potential of the fractions as wound healing therapeutics, samples were tested against gap-closure migration assays. Fractions that exhibit biological activity will be further evaluated and purified using HPLC [2].

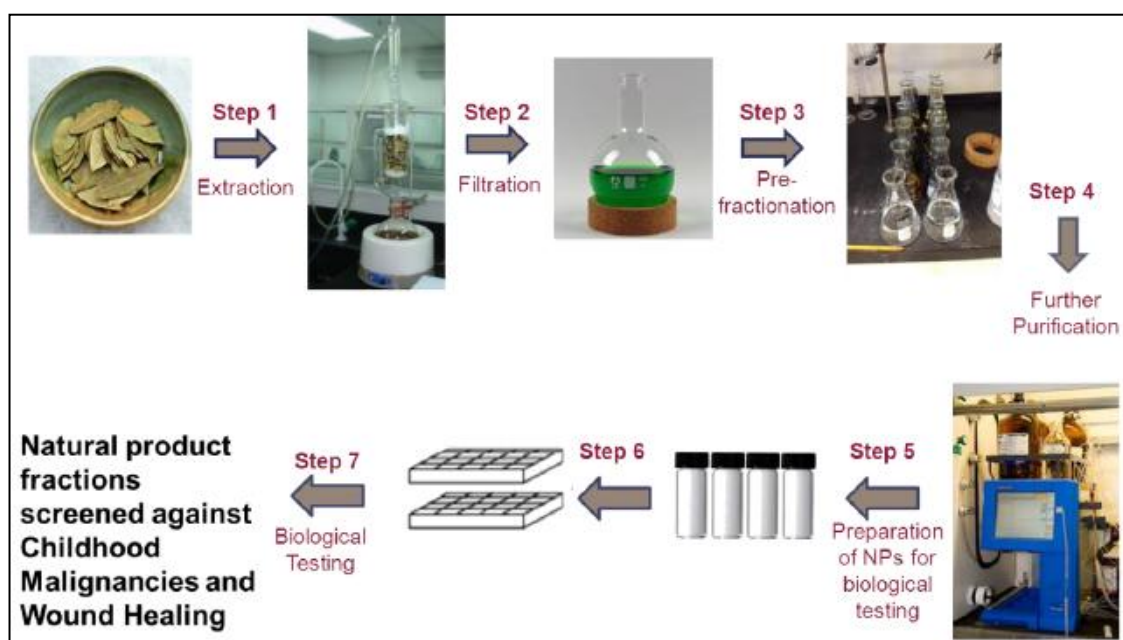


Figure 1: Bio-Guided Natural Product Drug Screening Platform

Based on preliminary biological results, we chose to evaluate the plant *Uncaria tomentosa* from the South American collection of natural products. This plant was of heightened intrigue because of its prevalent use in traditional medicine. *Uncaria tomentosa* is a medicinal plant found in the tropical jungles of Central and South America that has been used in folk medicine for its immunomodulatory, anti-cancer, and anti-inflammatory properties in addition to its ability to treat gastric ulcers, diarrhea, gonorrhea, arthritis and rheumatism, acne, diseases of the urinary tract, and a variety of cancers. Characterized as a woody, climbing vine belonging to the Rubiaceae family, *Uncaria tomentosa* contains unique curved hooks that contributed to its common name “uña de gato” or “cat’s claw” [3-5]. To evaluate this natural product as well as the others listed, we utilized a systematic extraction and pre-fractionation method illustrated in Figure 1.

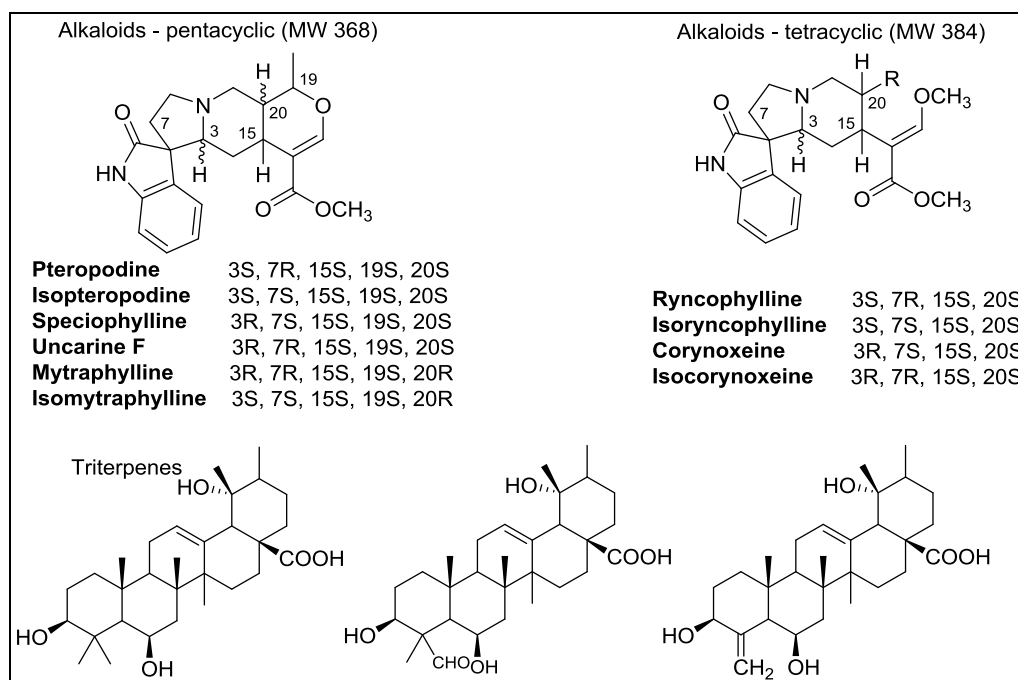


Figure 2: *Uncaria tomentosa* Natural Products Summary

Due to their therapeutic potential, the components of *Uncaria tomentosa* have been studied in great detail. A general summary of all of the secondary metabolites that have been reported from this plant is given in Figure 2. By definition, secondary metabolites serve no primary biochemical role in the plant but are produced for economic or defensive purposes. The specific compounds isolated from *Uncaria tomentosa* have been difficult to evaluate in great detail due to the fact that different isomers are isolated at different times of the year in various ratios depending on different stresses that the plant has experienced, particularly droughts. Further inconsistencies also exist based on the origin of the plant, thus complicating the execution of comprehensive studies of these natural products.

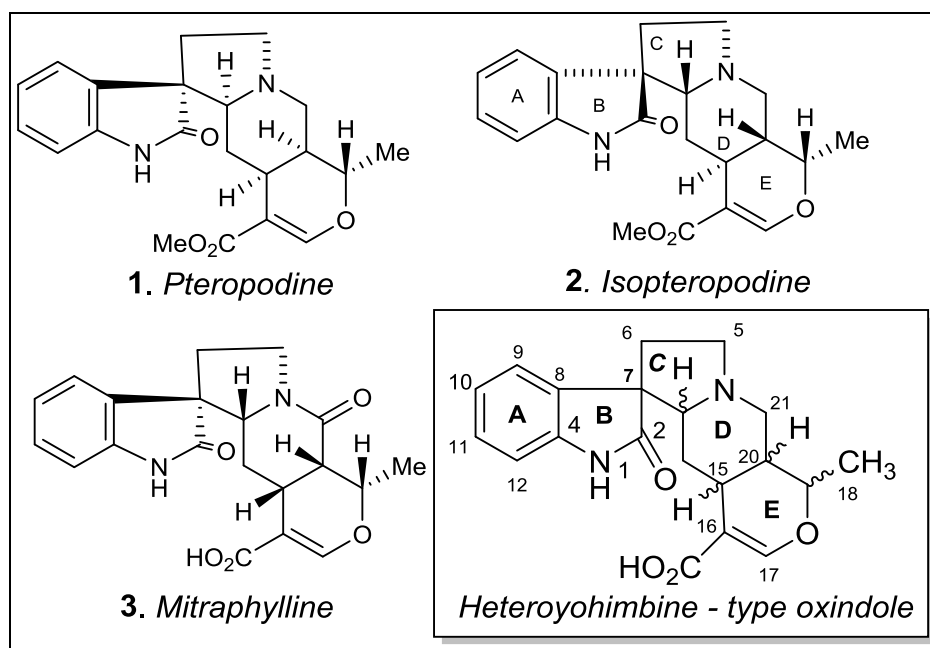


Figure 3: *Uncaria Tomentosa* Natural Products featuring Spirocylces

The key alkaloids isolated from *Uncaria tomentosa* are illustrated in Figure 3: pteropodine, isopteropodine, and mitraphylline. All of these alkaloids are

heteroyohimbine-type pentacyclic oxindoles that contain A, B, C, D, and E rings, the basic skeleton of which is boxed in Figure 3. The numbers on this boxed structure indicate respective carbon positions according to the general labeling method. The structural feature of the most interest to us was the key spirocenter joining the B and C rings at carbon 7. Spirocenters are defined as fully substituted atoms that join two organic molecules that are known as spirocycles and can be either all-carbon quaternary centers or tertiary centers. Spirocycles are present in numerous biologically active natural products, and clinically relevant compounds that can serve as molecular probes or therapeutic agents [6]. However, stereoselective and asymmetric methodologies to construct all carbon-carbon spirocenters remain scarce. Our goal in this project was to isolate pteropodine and develop methodologies to synthesize simplified oxindole compounds to be evaluated against a gap closure migration assay to develop potential therapeutics to treat impaired healing, specifically in diabetic and immunocompromised patients. We also aimed to explore the chemical space within the other pentacyclic oxindole alkaloids found in *Uncaria tomentosa*, which are known to possess wound healing properties due to the unique spirocenter structural feature.

Ene Reaction Approach to All-Carbon Spirocenters

We hypothesized that we could access simplified pteropodine-inspired all-carbon and indole spirocycles structures using an ene-type reaction. The ene reaction, or

Alder-ene reaction, has been described as “one of the most simple and potentially versatile reactions in organic chemistry, but remains surprisingly underexploited” [7]. A general ene reaction is a thermal reaction between an ene and enophile to form a new bond through migration of a new double bond and a [1,5]-hydrogen shift as illustrated in Figure 4. An ene is defined as an olefin containing an allylic H atom, and an enophile is an electron deficient double or triple bond that wants to react with the allylic hydrogen. During this pericyclic reaction, the double bond on the ene shifts and new C-H and C-C σ bonds are formed between the ene and enophile [8]. The mechanism of this Alder-ene reaction is quite similar to the allylic system of the Diels-Alder reaction, but in place of the Diels-Alder dienophile is the enophile of the ene reaction. Other differences arise in the higher temperature required by the Alder-ene reaction due to the higher activation energy and stereo-electronic requirement of breaking the allylic C-H bond of the ene.

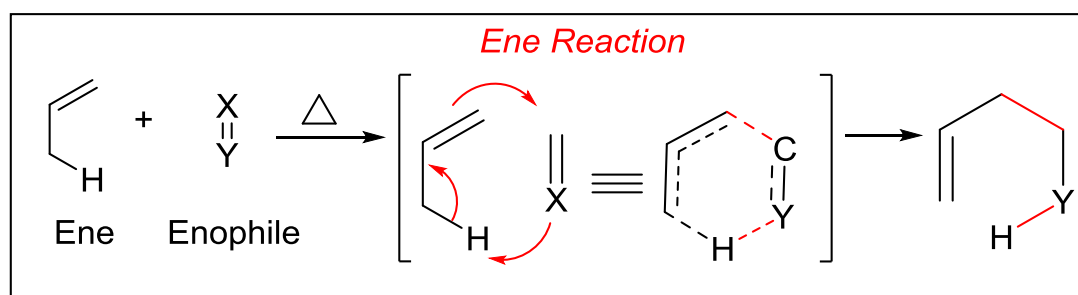


Figure 4: Proposed Ene Reaction Mechanism

In addition to the intermolecular Alder-ene reaction is the intramolecular Conia-ene reaction, a thermal or Lewis acid catalyzed reaction of an unsaturated carbonyl compound to yield a cyclic system. Similar to the Alder-ene reaction,

the Conia-ene reaction mechanism involves an enolization followed by a [1,5]-hydrogen shift. Advances involving the general ene reaction have been made by Andrew Kende and Koichi Mikami. Kende contributed to the ene reaction through his Pd(II) mediated synthesis of bridged and spirocyclic bicycloalkenones (Figure 5: Reaction 1) [9]. This facile synthesis suggested that Pd(OAc)₂-mediated cyclizations might serve as favored routes to bridged and spirocyclic bicycloalkenones even when competing conjugated enone formation is structurally possible [10]. While this novel synthesis advanced the capabilities of the basic ene reaction, they were not able to identify the full mechanism of their novel cyclizations leaving more to be discovered about this reaction. Mikami made advances toward the versatile ene reaction by introducing chirality to these spirocyclic structures. He developed a highly enantioselective intramolecular [4+2] cycloaddition reaction catalyzed by cationic chiral Rh complexes bearing not only a chiral phosphine but also a chiral diene (Figure 5: Reaction 2) [11]. Despite these advances, the ene reaction still requires significant activation for the reaction to take place. Mikami's reaction, while an advance on the ene reaction functionality, still requires an activated system with an allylic nitrogen. Milder conditions are needed to make the ene reaction more versatile and functional for synthetic chemists.

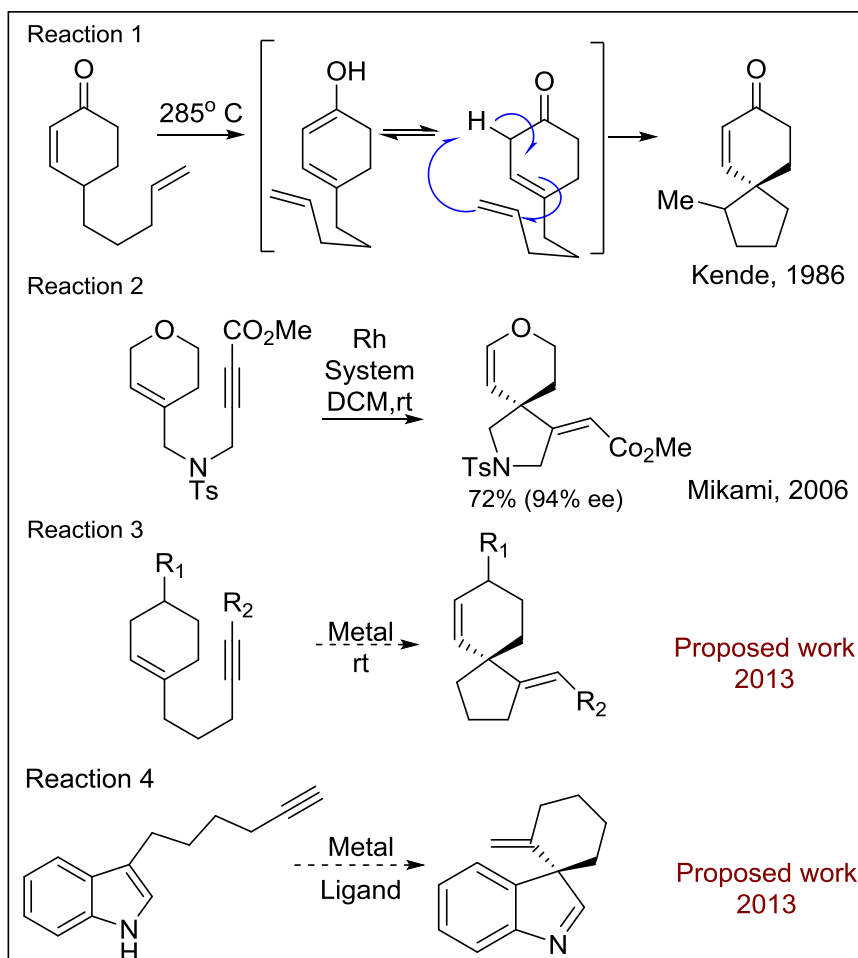


Figure 5: Advances on the Ene Reaction

Our hypothesized ene-type reaction sequence (Figure 5: Reaction 3) will expand the practical capabilities of the well-established ene reaction utilizing an unactivated, neutral system. We predict that this ene-type reaction will be successfully mediated by a metal catalyst instead of the harsh thermal conditions typical of an ene reaction to allow for various functional groups to be included. Such conditions will enable the ene reaction to produce compounds with a broad chemical space, like our proposed indole system (Figure 5: Reaction 4). These conditions have not been previously attempted for an ene-

type reaction and would be a novel addition to the capabilities of the ene reaction and a valuable tool for synthetic chemists. Additionally, the resulting spirocycles would allow chemists to synthesize various natural products and other complex, biologically active structures. Furthermore, the application of our spirocycles for wound healing presents a novel opportunity to explore the link between natural products and the wound-healing process.

Therapeutic Focus: Wound Healing

Based on the known healing properties of *Uncaria tomentosa* due to the unique properties of its pentacyclic oxindoles, we hypothesized that similar spirocycles will also be able to make advances in the general wound healing process, specifically for the patients severely affected by impaired healing. Wound healing is a complex process in which the skin or another tissue repairs itself after chemical or physical insult. In normal skin, the epidermis (outermost layer) and dermis (inner layer) exist in steady-state equilibrium, forming a protective barrier against the external environment. By definition, a wound is a “disruption of normal anatomic structure and function” that results from pathologic processes beginning internally or externally. The four phases of wound healing for healthy individuals are hemostasis, inflammation, proliferation or granulation, and remodeling or maturation [12]. In order for effective wound healing, proper sequence, specific timing, and appropriate duration must all occur precisely. Several systemic factors can affect a person’s ability to heal at a normal rate

including age, gender, disease, obesity, nutrition, and immune system conditions [13]. Specific diseases prone to delayed wound healing include diabetes, keloids, fibrosis, jaundice, and uremia. Immunocompromised patients, like those undergoing chemotherapy, radiation treatment, and AIDs patients, as well as those taking glucocorticoid steroids and non-steroidal anti-inflammatory medications, are also at increased risks for delayed wound healing. Non-healing wounds affect 3 to 6 million people in the United States, costing an estimated \$3 billion per year [13]. Therefore, the development of therapeutics that enhance wound healing could result in decreased hospitalization times as well as earlier return of patients to their daily functions. Such a wound healing therapeutic could allow for a potential savings of \$11 billion in total health care costs.

The wound healing process involves an intricate combination of signals and pathways to effectively close a wound. This process is often significantly disrupted or delayed in diabetic and immunocompromised patients who are commonly faced with impaired or delayed wound healing. Impaired healing is caused by pathologic inflammation due to an incomplete or uncoordinated healing process that may lead to infection and necrosis. Such delay in the wound healing process is the most common complication of diabetic patients due to poor glucose control and can take between 12 and 18 months to go to proper completion. A simple injury in these patients can rapidly become a serious infection, and require amputations to stop the infections from spreading (this is the leading cause of non-traumatic lower limb amputation in the United

States). Despite the significant need for effective therapeutic agents, very few treatments are in the drug development pipeline due to the complexity and poor understanding of the etiology of the disease [14]. When damage occurs to the epithelial cells the wound healing process initiated. This process includes “rapid hemostasis, appropriate inflammation, mesenchymal cell differentiation, proliferation and migration to the wound site. Following this is suitable angiogenesis, prompt re-epithelialization (or re-growth of skin tissues over the wound), proper synthesis, cross-linking, and alignment of collagen to provide strength to the healing tissue.”

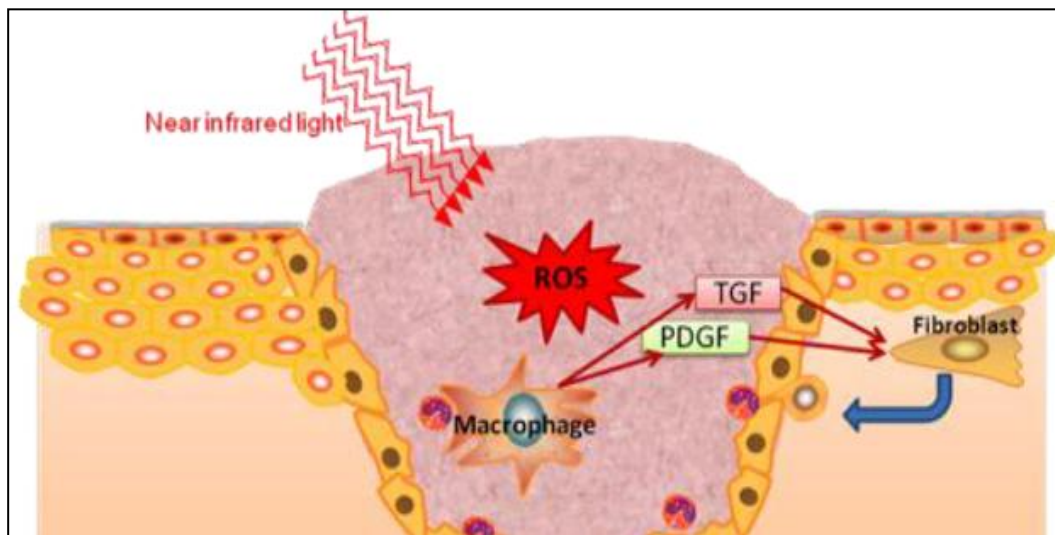


Figure 6: Role of Macrophages in Wound Healing.

Figure 6 depicts the various signals that initiate the wound healing process, specifically the role that macrophages play. The first stage in this process is inflammation, which causes the recruitment of macrophages to the site of the injury. Macrophages (Greek for “big eaters”) are white blood cells that are produced by differentiation of monocytes based on the type of stimuli received by

the tissue. Specifically, macrophages are involved in maintaining the tissue homeostasis of the wound healing process, including tissue surveillance and immunosuppression. Their main role is “constantly surveying their immediate surroundings for signs of tissue damage or invading organisms.” Macrophages function in both the innate and adaptive immunity of the body by engulfing and digesting cellular debris and stimulating immune cells [15]. There are three key types of macrophages involved in wound healing: cytotoxic, inflammatory, and repair. The macrophage known as cytotoxic, or “killer,” removes bacteria and other debris from the site of injury to help prevent infection. Another important macrophage, the inflammatory macrophage, is recruited by the presence of 1,3 β -glucan and is responsible for attracting fibroblasts, which synthesize the extracellular matrix and collagen, and endothelial cells that provide an anticoagulant barrier between the blood vessel wall and the blood. Once the inflammatory macrophage recruits these cells to the site of the wound, it encourages them to proliferate by producing platelet derived growth factor (PDGF), transforming growth factor β (TGF- β), and basic fibroblast growth factor. During this process, the fibroblasts produce hyaluronan, which causes the monocytes to differentiate into the final repair macrophages, whose function is to remodel the extracellular matrix of the wound [16]. Also shown in Figure 6 is the presence of reactive oxygen species (ROS), or “chemically reactive molecules formed by the partial reduction of oxygen,” in wound healing as the result of near infrared light. In normal wound healing, ROS are activated during the inflammation phase as a “natural byproduct of normal oxygen metabolism and

play a role in signaling and homeostasis.” However, in a delayed wound healing system, ROS can contribute to chronic inflammation and infections. As described, there are several ongoing processes in wound healing, making it difficult to target a single aspect; therefore, we will not attempt to pinpoint a specific molecular target but the entire process. We will take a broader screening approach to study how spirocycles might affect this wound healing process.

Objectives

Previous studies involving the systematic evaluation of *Uncaria tomentosa* extracts as potential wound healing therapeutics have been hindered by the significant differences in composition between samples. With our proposed ene-type reaction, we will be able to synthesize precursors of this biologically active complex system not previously accessible. Our synthesis of all-carbon and indole spirocycles has the potential to unlock facile synthetic routes to key spirocycles like those derived from *Uncaria tomentosa* as well as a wide variety of other natural products. We hypothesize that a modified ene-type reaction can be mediated by a metal complex under mild reaction conditions, thus tolerating a broad range of functionalities leading to unrestricted substrates. Our research strategy consisted of the following systematic approach:

Objective 1: We conducted a bio-guided screening approach of 14 natural products that led to the isolation, structure elucidation, and characterization of the pentacyclic oxindole pteropodine from the natural product *Uncaria tomentosa*. To

carry out an efficient drug discovery platform, we then conducted structure-activity relationship studies by making synthetic derivatives of pteropodine.

Objective 2: We evaluated a synthetic approach to simplified terpene and oxindole compounds bearing a spirocenter to mimic the structure of the biologically active pteropodine. We hypothesized that an ene-type reaction would mediate this formation and evaluated a series of transition metal complexes to understand how they mediate a potential carbocyclic formation for a terpene scaffold. Figure 7 illustrates the general goal of this aim to form a simple, unfunctionalized all-carbon spirocycle. We hypothesized that various transition metals and ligands would be able to mediate an ene-type reaction to form a variety of intermediates to yield 5, 6, and 7 member rings under mild conditions without the need for harsh conditions and/or activating functional groups. Transition metals studied include platinum, palladium, indium, and silver alone or in combination.

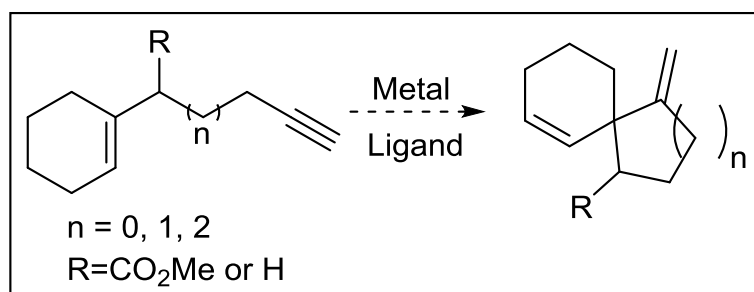


Figure 7: Proposed All-Carbon Spirocyclization Reaction (Model A)

To broaden the range of natural products accessible by the ene reaction we evaluated the formation of spirocenters on indole scaffolds to obtain the core of

oxindoles. Figure 8 highlights the proposed scheme for synthesizing indole spirocycles utilizing proven reactivity from the all-carbon spirocycles to gain access to structures similar to the heteroyohimbine-type pentacyclic oxindoles illustrated in Figure 3. With this advance, we will gain access to a broad range of natural products bearing key spirocenters through a relatively short synthesis.

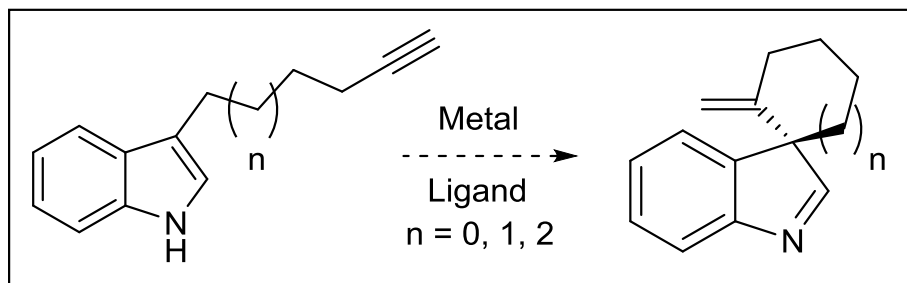


Figure 8: Proposed Indole Spirocyclization Reactions (Model B)

This approach included screening for metal catalysis, solvents, and ligands, allowing us to test for general activity, diastereoselectivity, and enantioselectivity respectively. Once we have achieved reactivity with a metal catalyst, we will evaluate a variety of solvents to optimize the reaction conditions. In addition, a library of ligands was evaluated to further optimize the reaction and gain access to a variety of other natural product-like structures.

Objective 3: The biological properties of the isolated natural products (objective 1) and simplified synthetic compounds featuring spirocenters (objective 2) will be tested using a scratch-wound healing, or cicatrisation, assay to identify potential therapeutic agents. Commercially available compounds with known wound healing properties will be used as controls.

Discussion and Results

Extraction, Isolation, and Structure Elucidation of Pteropodine

To begin evaluating pteropodine for its potential therapeutic effects, we extracted the *Uncaria tomentosa* plant material in 200 mL of isopropanol under reflux conditions. The extraction produced 10 g of extracts that were collected and stored under refrigeration conditions. The extracts were pre-fractionated by hand using a silica column with a solvent gradient ranging from 0 to 100% ethyl acetate in hexane followed by 0 to 20% methanol in dichloromethane. Seven fractions were collected based on solvent gradients and further purified individually on the Biotage Isolera 4 utilizing SNAP® 10 g cartridges. Each of the seven fractions produced a unique number of compounds whose structures were evaluated using 1 and 2 D NMR spectroscopy. These compounds of interest were evaluated for their biological activity as potential wound healing therapeutics on gap closure migration assays. The extraction process is summarized in Figure 1.

Figure 9 shows the compounds we isolated from the July and September collections of *Uncaria tomentosa* flowers. Pteropodine was not isolated in significant amounts from the July collection, and 200 mg were isolated from the September collection. Figure 9 illustrates the amounts of pteropodine isolated in comparison to other pentacyclic oxindoles present in the flower: isopteropodine, pteropodine, alkaloid A, and maruquine.

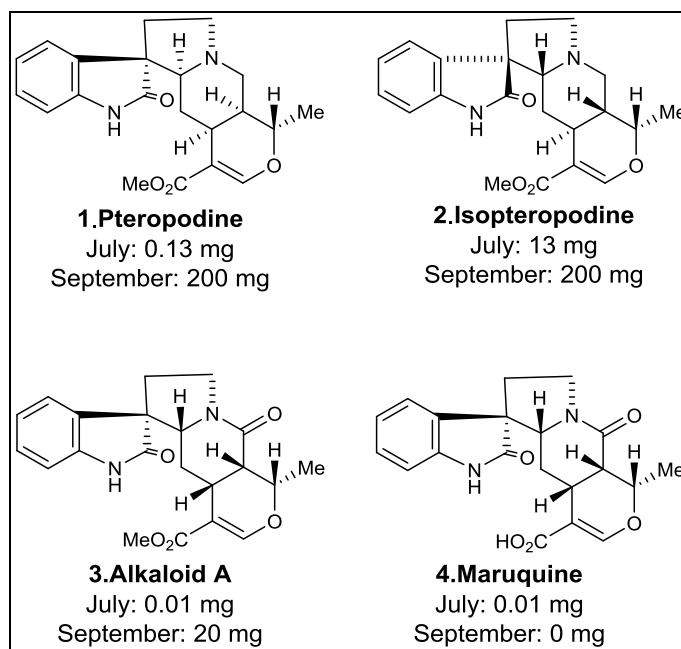


Figure 9: Isolated Ratio of Compounds from *Uncaria tomentosa*

The structure of pteropodine isolated from the fractionation of *Uncaria tomentosa* extracts was confirmed using a COSY experiment seen in Figure 10.

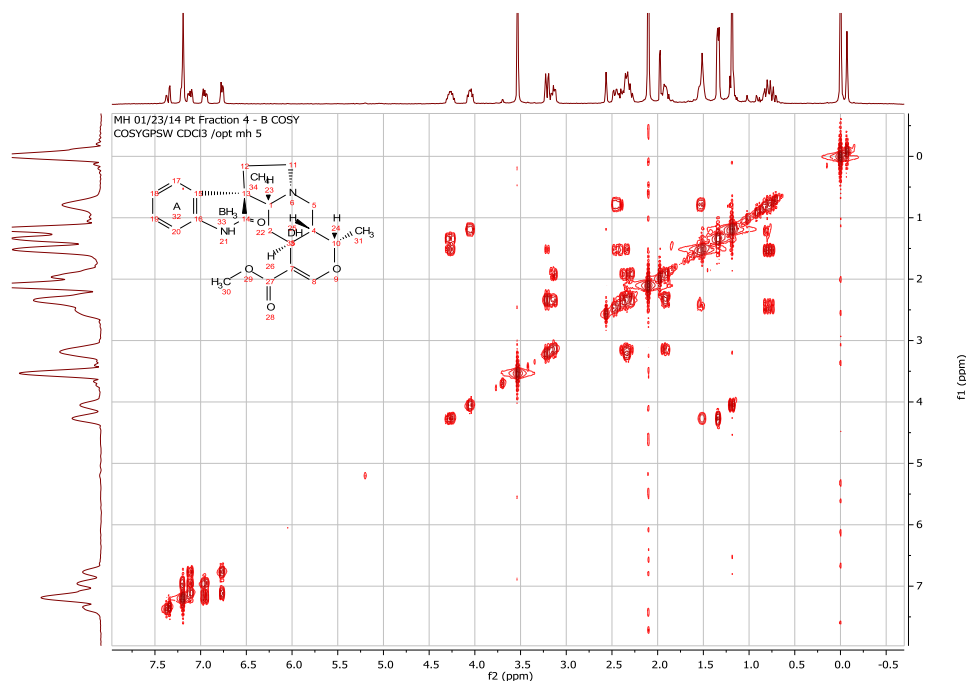
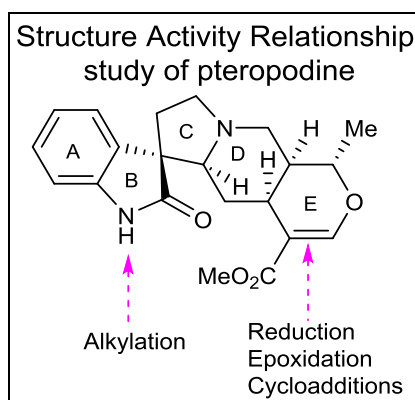


Figure 10: 2D characterization of pteropodine using COSY

Future Directions: Structure-Activity Relationship Evaluation of Pteropodine

The isolation and structure elucidation of pteropodine from the *Uncaria tomentosa* extracts will allow for future structure activity relationship (SAR) studies to better understand its functionality. This polycyclic natural product possesses five rings, and two of these rings can be further manipulated through synthesis. The indole can be alkylated with various groups to probe steric factors, whereas the E ring with its unique α,β -unsaturated system can potentially undergo cycloaddition reactions, halogenations, reductions, and epoxidations. At least, four synthetic analogues can be synthesized on the highlighted sites shown in scheme 1. The analogues will provide the rationale behind the activity of the natural product as a wound healing agent.

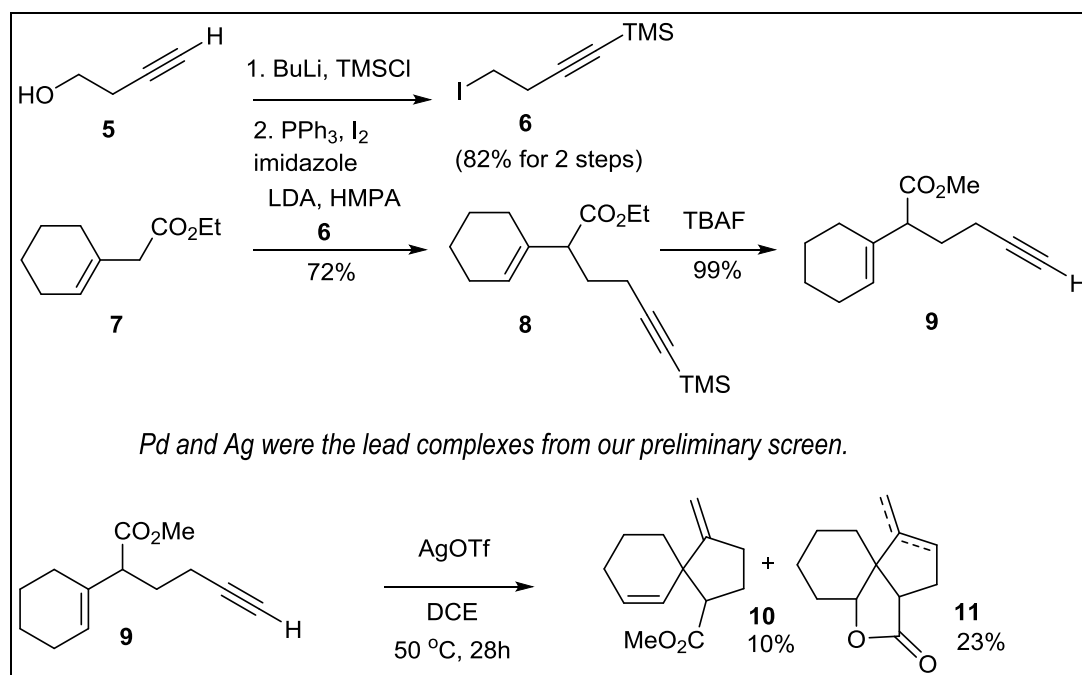


Scheme 1: Structure-Activity Relationship Evaluation of Pteropodine

Ene Reaction Model Study A: All-Carbon Spirocyclic Compounds

We began our ene reaction studies by synthesizing an all-carbon spirocycle. After exploring the initial reactivity potential of the Pd (II) mediated reaction, we expanded on this information and optimized the solvent system as well as other

catalysts. Once the conditions were sufficiently optimized, we utilized this known reactivity to form spirocycles from an indole core. After we have achieved promising synthetic routes, we tested the all-carbon and indole spirocycles for their biological activity in assisting the wound healing process via gap closure migration assays.



Scheme 2: Synthesis of Key Intermediate **9** and Promising Lead Reaction Conditions for All-Carbon Spirocycles

Scheme 2 illustrates the synthesis of key precursor **9**, which will allow us to test our hypothesis for the formation of all-carbon spirocycle **10**. The synthesis of precursor **9** began with the formation of the side-chain **6**. This was achieved from compound **5** by first protecting the alkyne with tetramethylsilane (TMS) followed by the iodination of the hydroxyl group. Side chain **6** was coupled with the core **7** via lithium diisopropylamide (LDA), a strong bulky base, and the polar aprotic solvent hexamethylphosphoramide (HMPA) to increase selectivity and

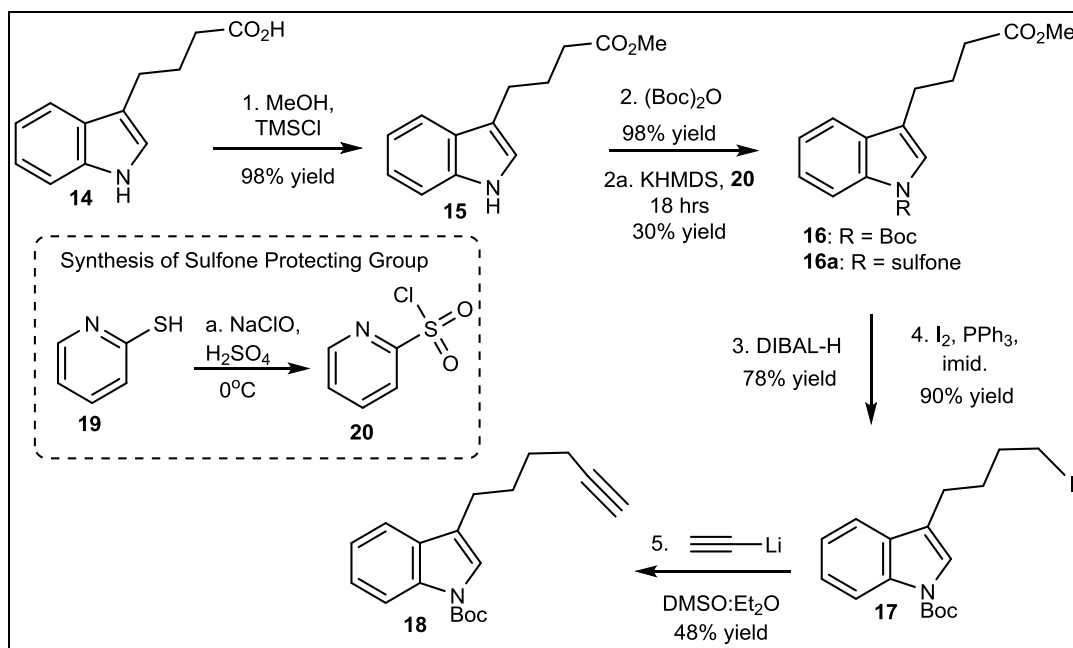
produce the protected compound **8**. The TMS protecting group was cleaved by tetrabutylammonium fluoride (TBAF) to yield precursor **9**, allowing us to begin screening cyclization conditions for the all-carbon system. Experimental details and characterization via NMR studies is included in the supporting information.

After the core was successfully synthesized, we began our studies by evaluating the ability of various transition metals to mediate the formation of an all-carbon spirocycle. Metal catalysts including platinum, palladium, indium, and silver were evaluated. We explored a variety of solvents and catalysts to obtain optimized reactivity to form these spirocenters. Scheme 2 illustrates the results of our optimized conditions for the synthesis of these all-carbon spirocycles via an intramolecular ene-type reaction. Spirocycle **10** was formed utilizing key intermediate **9** and silver trifluoromethanesulfonate (AgOTf) as a catalyst in dichloroethane (DCE). The reaction proceeded at a mild temperature (50°C) but only in poor yields of 10%. However, the ability of this ene-type reaction to successfully proceed is very promising for further screening of conditions as well as for the formation of an indole system.

Ene Reaction Model Study B: Indole Spirocyclic Compounds

With the success of forming the all-carbon spirocycles **10** and **11** from model studies A, we began synthesizing the core for the indole system. Scheme 3 illustrates the synthetic route used to afford the key intermediate **18** for the indole spirocycles. This synthesis commenced with the esterification of

commercially available butyric acid **14** via catalytic amounts of trimethylsilyl chloride (TMSCl) producing compound **15** in 98% yield. The protection of the nitrogen was a crucial step.



Scheme 3: Synthesis of Precursor 18

Due to the unique chemical properties of indoles and their basicity, protecting compound **15** presented a range of potential complications [12]. If left unprotected, the nitrogen could coordinate with the metal catalyst, potentially inhibiting the reaction since we are only dealing with catalytic amounts of the metal. It is crucial that we chose an appropriate protecting group because the protecting group itself has the potential to interfere in the reaction mechanism. The protecting group could coordinate with the catalytic metal, which would block overall reactivity. Furthermore, the protecting group could cause steric hindrance and aromaticity effects, thus blocking activity of the cyclization. For these reasons we prepared both the carbamate protected compound **16** with

Boc (tert-butyloxycarbonyl) and the sulfonamide protected compound **16a**. Due to its “umbrella” like structure, the carbamate has the potential to inhibit the reaction by causing steric hindrance for the cyclization. If this is the case, the sulfonamide’s flat structure and decreased electron withdrawing capabilities should provide a viable core for cyclization. This alternative core utilizes the protecting group N-(2-pyridyl) sulfonyl chloride [11]. This protecting group was boasted to be easily installed and capable of exerting complete regiocontrol over the Pd(II) catalyzed C-H bond. If the Boc-protected compound **18** presents difficulties in the formation of a spirocycle, we have compound **16a** to go back to and synthesize an alternate core for this indole system. The synthetic route for the formation of compound **16a** is illustrated in Scheme 3. We synthesized protecting group **20** from 2-mercaptopyridine, **19**, using sodium hypochlorite and concentrated sulfuric acid. This protecting group **20** was added to methyl ester **15** via KHMDS (potassium bis(trimethylsilyl)amide) producing our back-up intermediate **16a**. The percent yield for this protection was not ideal, so further evaluation is needed to optimize this reaction.

The Boc protected methyl ester **16** underwent a DIBAL-H (diisobutylaluminum hydride) reduction at -78°C, yielding the primary alcohol 78% yield with 22% recovered starting material, **16**. The primary alcohol underwent iodination producing compound **17** in 90% yield, which produced the Boc-protected key intermediate alkyne **18** via neat lithium acetylide. All reactions were carried out on a multi-gram scale, under inert atmosphere, and monitored by thin layer

chromatography and mass spectroscopy. All final compounds were purified and characterized using nuclear magnetic resonance. These spectra are included in the supporting information.

Once we established successful reactivity of the ene reaction from intermediate **18** to the indole spirocycle **21** using a metal catalyst (Table 2), we screened solvents and ligands to create the most effective synthesis to gain access to a broad range of natural-product-like spirocycles with known wound healing properties. A brief summary of catalyst screening conditions is given in Table 2. Catalysts screened include silver triflate (AgOTf), indium triflate (InOTf), scandium triflate (ScOTf), tetrakis(acetonitrile) palladium(II) tetrafluoroborate ($[\text{Pd}(\text{MeCN})_4](\text{BF}_4)_2$), magnesium perchlorate ($\text{Mg}(\text{ClO}_4)_2$), zinc chloride (ZnCl_2), and a combination of silver and indium triflate. The most promising metal catalyst proved to be the combination of silver and indium triflate. Unfortunately, good yielding reaction conditions have yet to be identified. The reaction proceeds under Lewis acid activation namely, Indium in combination with silver triflate as illustrated in Table 2. However, the yields are rather low, and the reaction does not proceed to completion. In addition, the retention time of the product and starting material does not differ complicating the monitoring of the reaction by TLC. Mass spectroscopy is also ambiguous since both starting material and parent compound share the same chemical mass. NMR is the only experimental approach to follow the reaction and it still needs careful evaluation since the metals cause small shifting in the magnetic field, the reaction mixture

needs to be purified via column chromatography and high performance liquid chromatography (HPLC) in order to properly isolate and identify the product.

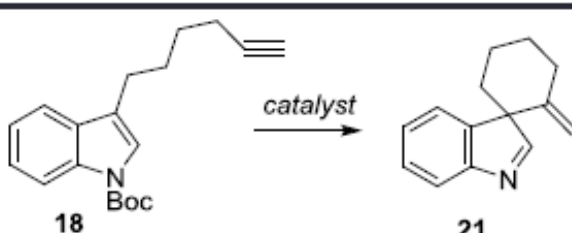
Table 2: Results of Screening Conditions for Model B Compounds		
		
entry	catalyst	result
1	AgOTf	No Reaction
2	In(OTf) ₃	Boc Deprotection
3	Sc(OTf) ₃	Boc Deprotection
4	[Pd(MeCN) ₄](BF ₄) ₂	Complex Mixture*
5	Mg(ClO ₄) ₂	No Reaction
6	ZnCl ₂	Complex Mixture*
7	AgOTf/ In(OTf) ₃	(~20%) chemical yield
*Complex mixture indicates a mixture of cyclized isomers, Boc deprotected starting material, reduction of the alkyne, and polymerized products.		

Table 2: Results of Screening Conditions for Model B Compounds

Biological Studies via Cicatrisation Assays

In order to test the biological activity of the generated molecules, we utilized an established gap closure migration assay to determine the compounds' ability to promote cicatrisation, or wound healing. The general principle behind this *in vivo* study is to create a wound or gap in the cells and observe how the cells migrate to fill the gap. Figure 11 illustrates the general procedure for the gap-closure migration assay. Steps followed include: developing a confluent cell monolayer,

creating a “wound” by scratching the cells with a sterile pipette tip, and observing how the cells migrate to fill the wound over time. We used commercially available natural products with known wound healing properties to provide a basis for comparison with our compounds. The preliminary cell line to be studied is the MDA-MB231 aggressive breast cancer cell line. This cell line exhibits the most migratory behavior that we have observed, and testing our compounds against such a well-documented and rapidly migratory cell line enabled us to optimize the assay to be able to test against additional cell lines including MCL7, macrophage 677.1, and STO, as they are acceptable model systems for wound healing. In order to conduct these assays, we will place a wound healing insert in a cell suspension and allow the cells to form a confluent monolayer around the insert. Using this insert allows us to create a consistently defined 0.9mm wound gap, reducing inter-sample variation common among other methods. When the insert is removed, a wound gap is created, and cells can then be monitored for proliferation or migration across the wound field. Cell migration can be monitored by imaging samples at fixed time points or by time-lapse microscopy [17].

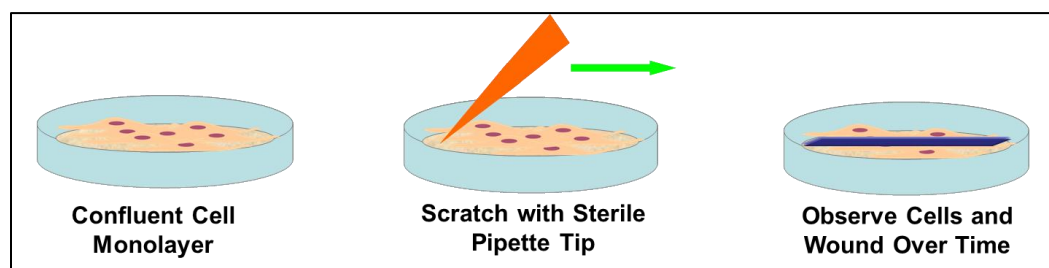


Figure 11: Gap-Closure Migration Assay

Cells will continue to migrate across the wound until the wound field is completely closed. The rate of wound closure between control and treated cells will allow us to determine the efficacy and potential therapeutic relevance of the generated compounds [18]. An increased “healing” in reference to control or untreated cells is anticipated due to the known wound healing properties of the similar spirocycles found in *Uncaria tomentosa*. Such an increase will indicate that that our compounds can assist in the wound healing process, potentially for the diabetic and immunocompromised patients previously described.

Tables 3 and 4 outline the compounds that were tested against the MDA-MB-231 gap-closure migration assay. Table 3 lists the compounds from the *Uncaria tomentosa* extraction, the all-carbon spirocycle synthesis, and intermediates in the indole synthesis.

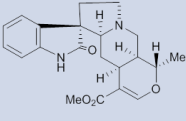
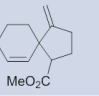
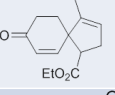
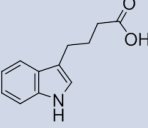
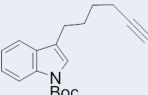
Number	Origin	Structure
1	<i>Uncaria tomentosa</i> Fraction 4 – Compound B (Pteropodine)	
1a	<i>Uncaria tomentosa</i> Fraction 1 – Compound A	
10	All Carbon Spirocycle	
22	All Carbon Spirocycle	
14	Indole Precursor	
18	Indole Key Intermediate	

Table 3: List of Compounds Tested via Migration Assay

Compound **1** was isolated from the fourth fraction of *Uncaria tomentosa* extracts and structure elucidation proved the compound to be pteropodine. Similarly, compound **1a** was isolated from the first fraction of *Uncaria tomentosa* extracts and its structure was elucidated via ^1H , ^{13}C , and 2D NMR studies. All carbon spirocycles **10** and **22** were tested for their potential as wound healing agents, as well as key intermediates **14** and **18** from the indole Model B system. Compound **22** was previously synthesized in lab via the same reaction conditions as compound **10** and was included in our wound healing study as a reference of a functionalized all-carbon spirocycle. There was not enough material generated of the cyclized indole compound **21** to submit for biological testing. Table 4 characterizes the controls that were used in the migration assay. The natural products *Rhodiola crenulata* (*R. crenulata*) and curcumin have documented wound healing inhibition properties; therefore, we used these two compounds for negative controls for our studies. Additionally, all compounds submitted for biological testing were in a 50 μM solutions of DMSO, so a sample of 0.05% DMSO was used to simulate a positive control, or untreated cells. The positive controls were made in solutions of EtOH, thus the 0.1 % EtOH treated cells indicate the untreated cells corresponding to these controls.

Controls	Reference
<i>R. Crenulata</i>	Negative Control
Curcumin	Negative Control
0.1% EtOH	Vehicle
0.05% DMSO	Vehicle

Table 4: List of Controls for Migration Assay

Figure 12 summarizes preliminary biological results of select compounds tested against a gap-closure migration, or cicatrisation, assay as line graphs quantifying the effect of the compounds on cell migration. Plotted along the x-axis is the time progression of the assay in hours. The y-axis shows the relative wound density as a percentage of the scratch that has been closed. The confluence, or relative area covered by the cells, of the scratch-wound was observed over a period of 48 hours.

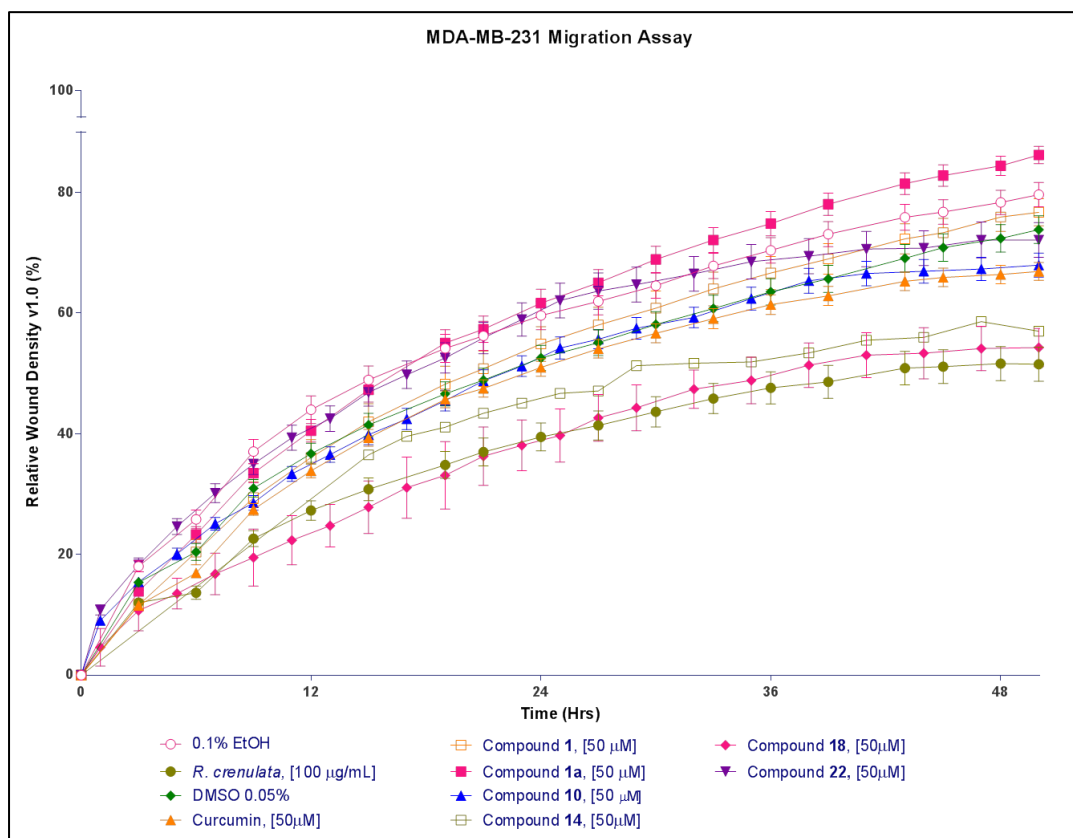


Figure 12: Migration Assay Results

As shown in Figure 12, compounds **1** and **1a** exhibited accelerated wound healing in comparison to the DMSO control. Treatment with all-carbon spirocycle **10** exhibited wound healing at a rate similar to the curcumin control, and

spirocycle **22** initially exhibited accelerated wound healing but that rate leveled off in a similar manner to the DMSO control after 42 hours. Indole compounds **14** and **18** inhibited cell migration comparable to the *R. crenulata* control. Such inhibition offers the opportunity to use these compounds as anti-metastases therapeutic agents. These preliminary results indicate compounds **1** and **1a** have potential as wound healing therapeutics. Additional studies are needed to confirm these results as well as better quantify the effects of the all-carbon and indole compounds.

The migration of the cells was recorded as pictures via the Essen Bioscience IncuCyte. These still images were taken every hour up to 48 hours post-scratch and qualitatively depict how the cells treated with compounds **1**, **1a**, **10**, **22**, and **14** migrated across the scratch in comparison to the DMSO control. Due to the presence of technical artifacts, these results are indicative of the compounds' preliminary potentials as therapeutic agents, but are not conclusive.

Conclusions

Objective 1: We were able to efficiently process fourteen natural products (*Hydrastis Canadensis*, *Quercus dumosa*, *Aristolochia leuconeura*, *Phacelia hastate*, *Acer rubrum*, *Oenanthe sarmentosa*, *Salvia mellifera*, *Terminalia catappa*, *Uncaria tomentosa*, *Onoclea sensibilis*, *Ligusticum cf. grayi*, *Dioscorea evbulbifera*, *Cuphea hyssopifolia*, and *Solanum sisymbriifolium*) through a bio-guided drug discovery process. This led to the subsequent extraction, isolation, and structure elucidation of 200 mg of pteropodine, the structural inspiration for our ene-reaction studies.

Objective 2: An ene-type reaction scheme was evaluated against all-carbon and indole systems. Intermediates **9** and **18** were synthesized in excellent yields to allow for the evaluation of cyclization conditions including metal catalysis, solvents, and ligands to test for general activity, diastereoselectivity, and enantioselectivity. All-carbon spirocyclization conditions were realized in compound **10** in 10% yield allowing for the continuation and further evaluation of reaction conditions. Additionally, conditions were discovered to achieve cyclization of indole **18** to form compound **21** in 20% yield. These results indicate promise for further functionalization and utilization of an ene-type reaction to achieve a wide range of natural products whose structures feature a common spirocenter.

Objective 3: Preliminary biological results indicate that compounds **1** and **1a** isolated from *Uncaria tomentosa* exhibit increased migration of cells across a scratch-wound indicating their potential as wound healing therapeutics.

Supporting Information

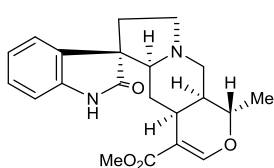
Synthetic procedures and compound characterization

Reagents of the highest available quality were purchased and used without further purification unless otherwise stated. Reactions were monitored by thin-layer chromatography (TLC) carried out on 0.25 mmol E. Merck silica gel plates (60F-254) using UV light for visualization and an ethanolic solution of anisaldehyde and heat as developing agents. Reactions were also monitored by using Agilent 1100 series LCMS and a low-resonance electrospray model (ESI) with UV detection at 25nm. Title compounds were purified by flash column chromatography using E. Merck silica gel (60, particle size 0.040–0.063 mmol) or Biotage Isolera Four with normal-phase silica gel. ^1H and ^{13}C NMR spectra were recorded on a Bruker (AV-400 or DRX-500 MHz) NMR spectrometer instruments calibrated with residual undeuterated solvent (CDCl_3 : $\delta_{\text{H}} = 7.26$ ppm, $\delta_{\text{C}} = 77.16$ ppm; acetone- d_6 : $\delta_{\text{H}} = 2.05$ ppm, $\delta_{\text{C}} = 29.84$ ppm; CD_3CN : $\delta_{\text{H}} = 1.94$ ppm, $\delta_{\text{C}} = 1.32$ ppm; CD_3OD : $\delta_{\text{H}} = 3.31$ ppm, $\delta_{\text{C}} = 49.00$ ppm; $\text{DMSO}-d_6$: $\delta_{\text{H}} = 2.50$ ppm, $\delta_{\text{C}} = 39.5$ ppm; D_2O : $\delta_{\text{H}} = 4.79$ ppm) as an internal reference. The following abbreviations were used to designate the multiplicities: s=singlet, d=doublet, dd=double of doublets, t=triplet, q=quartet, m=multiplet. Purity of final compounds was >95% based on analytical HPLC and NMR analysis. Yields refer to chromatographically and spectroscopically (^1H NMR) homogeneous materials.

Extraction and Isolation of Pteropodine from *Uncaria tomentosa*

Uncaria tomentosa plant material was extracted with a Soxhlet apparatus in 200 mL of isopropanol under reflux conditions for two days. The isopropanol solution

was filtered, and the remaining plant material was re-extracted for an additional two days. After decanting the solution from the remaining plant material, the two solutions were combined and concentrated. The extraction produced 10 g of extracts that were collected and stored under refrigeration conditions. The extracts were pre-fractionated by hand using a silica column with a solvent gradient ranging from 0 to 100% ethyl acetate in hexane followed by 0 to 20% methanol in dichloromethane. Seven fractions were collected based on solvent gradients and further purified individually on the Biotage Isolera 4 utilizing SNAP 10 g cartridges. Each of the seven fractions produced a unique number of compounds whose structures were evaluated using 1 and 2 D NMR spectroscopy.



Pteropodine (**1**)

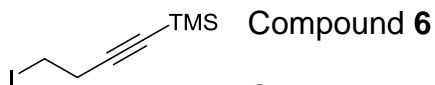
Yellow solid; ^1H NMR (400 MHz, Chloroform-*d*) δ 7.55 (s, 1H), 7.41 (d, $J = 2.3$ Hz, 1H), 7.21 – 7.15 (m, 1H), 7.02 (ddd, $J = 9.8, 7.1, 2.3$ Hz, 1H), 6.84 (dd, $J = 7.7, 2.4$ Hz, 1H), 4.34 (dd, $J = 10.5, 5.9$ Hz, 1H), 3.31 – 3.19 (m, 2H), 2.55 – 2.29 (m, 6H), 2.12 – 1.91 (m, 3H), 1.64 – 1.53 (m, 6H), 1.29 – 1.22 (m, 6H), 0.93 – 0.82 (m, 3H). ^{13}C NMR (126 MHz, CDCl_3) δ 179.64, 166.60, 153.97, 138.89, 132.70, 126.67, 123.65, 121.59, 108.81, 108.34, 76.24, 76.19, 75.99, 75.74, 71.13, 70.34, 55.77, 53.14, 52.50, 49.97, 36.86, 33.83, 29.45, 29.16, 28.25, 17.63, 0.00, -1.02.

Isolated Compound (**1a**)

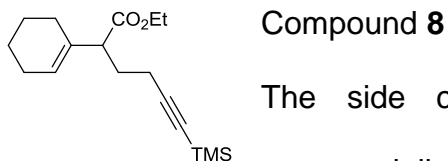
White solid; ^1H NMR (400 MHz, Chloroform-*d*) δ 5.11 (dp, $J = 13.4, 6.7, 6.2$ Hz, 1H), 4.17 – 3.97 (m, 0H), 2.02 (ddp, $J = 31.5, 12.7, 6.7, 5.9$ Hz, 4H), 1.63 (dd, $J =$

31.7, 5.1 Hz, 4H), 1.28 – 1.16 (m, 2H), 0.97 (d, $J = 6.5$ Hz, 0H), 0.86 (qd, $J = 7.0$, 2.3 Hz, 1H). ^{13}C NMR (101 MHz, CDCl_3) δ 135.10, 134.89, 131.24, 124.41, 124.30, 124.27, 77.33, 77.01, 76.69, 39.76, 39.74, 31.60, 28.28, 26.78, 26.67, 25.70, 25.37, 22.66, 17.68, 16.04, 16.00, 14.12.

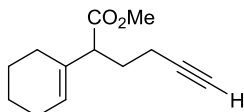
Synthesis of All-Carbon Compounds



Compound **6** was achieved from the commercially available compound **5** (but-3-yn-1-ol). First, the alkyne of compound **5** was TMS protected using butyllithium (BuLi) and trimethylsilane chloride (TMSCl). This protected compound underwent iodination of the hydroxyl group using triphenylphosphine (PPh_3), iodine (I_2), and imidazole for an overall yield of 82% for both steps. ^1H NMR (400 MHz, Chloroform- d) δ 3.22 (t, $J = 7.5$ Hz, 1H), 2.79 (t, $J = 7.5$ Hz, 1H), 0.16 (s, 4H).



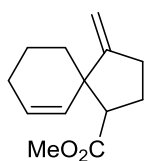
The side chain (compound **6**) was coupled with the commercially available core ethyl-2-(cyclohex-1-en-1-yl)acetate (compound **7**) using lithium diisopropylamide (LDA) as a strong base and hexamethylphosphoramide (HMPA) as a polar aprotic solvent to produce compound **8** in 72% yield. ^1H NMR (400 MHz, Chloroform- d) δ 5.61 (s, 1H), 3.68 (t, $J = 0.9$ Hz, 16H), 3.09 (s, 2H), 2.95 (s, 3H), 2.23 – 2.14 (m, 5H), 2.06 – 1.83 (m, 16H), 1.67 – 1.46 (m, 27H), 0.97 (dd, $J = 6.5, 0.7$ Hz, 2H), 0.15 (d, $J = 0.7$ Hz, 33H).

Compound **9**

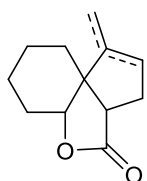
The TMS protecting group from compound **8** was cleaved by tetrabutylammonium fluoride (TBAF) to yield compound **9** in 99% yield. ^1H NMR (400 MHz, Chloroform-*d*) δ 5.63 (ddd, $J = 2.5, 1.8, 1.0$ Hz, 1H), 5.58 – 5.53 (m, 0H), 3.68 (s, 6H), 3.12 (s, 1H), 2.95 (dd, $J = 1.5, 0.8$ Hz, 1H), 2.20 – 2.13 (m, 2H), 2.07 – 1.89 (m, 9H), 1.84 – 1.73 (m, 1H), 1.68 – 1.50 (m, 8H), 0.97 (d, $J = 6.6$ Hz, 1H).

Compounds **10** and **11**

Compounds **10** and **11** were formed by the intramolecular cyclization of compound **9** via catalysis by AgOTf in DCE. Compound **10** as formed in 10% yields, and compound **11** was formed in 23% yield.

Compound **10**

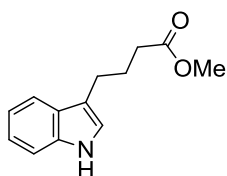
^1H NMR (400 MHz, Chloroform-*d*) δ 5.59 (s, 4H), 5.07 (d, $J = 1.3$ Hz, 1H), 4.93 (s, 1H).

Compound **11**

^1H NMR (400 MHz, Chloroform-*d*) δ 5.85 – 5.78 (m, 1H), 5.55 – 5.49 (m, 1H), 5.41 (dp, $J = 3.1, 1.6$ Hz, 1H), 4.39 (dd, $J = 9.7, 6.5$ Hz, 0H), 4.19 (dd, $J = 8.1, 5.5$ Hz, 1H), 3.80 – 3.58 (m, 1H), 2.88 (dd, $J = 6.7, 1.1$ Hz, 1H), 2.70 – 2.59 (m, 2H), 2.59 – 2.51 (m, 0H), 2.32 (tt, $J = 6.3, 4.3$ Hz, 0H), 2.19 – 2.07 (m, 1H), 2.05 – 1.92 (m, 3H), 1.81 – 1.62 (m, 6H), 1.63 – 1.51 (m, 4H), 1.51 – 1.45 (m, 1H), 1.42 (dd, $J = 9.4, 2.8$ Hz, 1H), 1.40 (s, 0H). ^{13}C NMR (101 MHz,

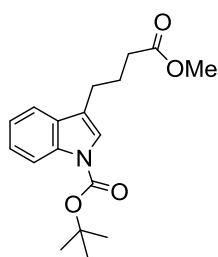
CDCl_3) δ 178.47, 130.84, 128.78, 82.22, 42.44, 41.61, 32.53, 28.26, 22.06, 21.54, 20.97, 18.25.

Synthesis of Indole Compounds



Compound **15**

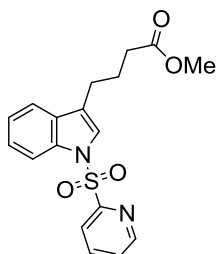
Commercially available butyric acid (5.0 g, 24.6 mmol) was combined with excess methanol (50 mL) at 50°C. A catalytic amount of TMSCl was added dropwise to the reaction mixture (0.63 mL, 4.92 mmol) and the reaction was monitored by TLC and allowed to proceed overnight. The reaction was quenched at room temperature with 0.5 mL of Et_3N (triethyl amine), the solvent was evaporated, and the compound was filtered with activated carbon.



Compound **16**

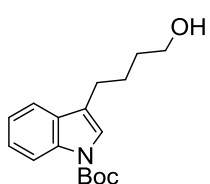
Compound **16** (3 g, 13.8 mmol) was dissolved in a 30 mL 1:1 solution of TEA and DCM at 0°C. To this solution, $(\text{BOC})_2\text{O}$ (6 g, 27.6 mmol) and a catalytic amount of DMAP (50 mg) were added. After 1 hour, the reaction was allowed to reach room temperature. Reaction progress was monitored by TLC and went to completion after 4 hours. ^1H NMR (400 MHz, CDCl_3) δ 8.15 – 8.07 (d, J = 8.0 Hz, 1H), 7.55 – 7.50 (ddd, J = 7.6, 2.4, 1.3 Hz, 1H), 7.39 – 7.35 (s, 1H), 7.33 – 7.27 (m, 1H), 7.25 – 7.19 (m, 1H), 2.78 – 2.69 (m, 2H), 2.45 – 2.36 (td, J = 7.3, 2.1 Hz, 2H), 2.07 – 2.01 (m, 2H), 1.71 – 1.62 (d, J = 2.1 Hz, 8H), 1.59 – 1.53 (d, J = 2.7 Hz, 1H). ^{13}C NMR

(101 MHz, CDCl₃) δ 173.74, 149.70, 135.55, 130.51, 124.26, 122.52, 122.31, 120.05, 118.93, 115.21, 83.24, 77.48, 77.16, 76.84, 51.42, 33.46, 28.15, 24.41, 24.21.



Compound **16a**

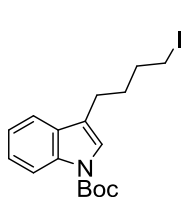
Compound **15** (100 mg, 0.46 mmol) was dissolved in 2 mL of anhydrous THF. KHMS (3.68 mL, 1.84 mmol) was added to this solution at 0°C and allowed to stir for 30 minutes. To this solution, compound **20** (106 mg, 0.60 mmol) was added, and the reaction mixture was brought to room temperature. The reaction was monitored by TLC and allowed to stir overnight. The reaction mixture was purified using a SNAP 10 g Biotage column. ¹H NMR (400 MHz, Chloroform-*d*) δ 8.59 (s, 1H), 8.01 (s, 1H), 7.91 (d, *J* = 1.9 Hz, 1H), 7.58 (t, *J* = 6.9 Hz, 2H), 7.51 – 7.40 (m, 3H), 7.19 (q, *J* = 7.0 Hz, 3H), 7.07 (dt, *J* = 15.6, 7.4 Hz, 3H), 6.84 (q, *J* = 3.0 Hz, 1H), 5.29 (d, *J* = 6.5 Hz, 4H), 4.54 (ddd, *J* = 10.2, 6.6, 3.7 Hz, 1H), 3.77 – 3.59 (m, 8H), 2.80 (p, *J* = 7.3 Hz, 3H), 2.45 – 2.38 (m, 2H), 1.85 (dd, *J* = 14.7, 7.1 Hz, 3H), 1.71 (dq, *J* = 9.2, 4.5, 3.4 Hz, 3H), 1.60 (q, *J* = 5.0 Hz, 3H), 1.50 (ddd, *J* = 11.4, 8.0, 5.0 Hz, 4H), 1.44 – 1.39 (m, 2H), 0.95 (t, *J* = 6.5 Hz, 5H). ¹³C NMR (101 MHz, CDCl₃) δ 150.21, 137.97, 136.49, 127.63, 123.38, 122.25, 122.17, 119.48, 118.79, 111.23, 100.07, 77.48, 77.41, 77.27, 77.16, 77.10, 76.84, 76.78, 66.39, 60.55, 53.00, 26.37, 22.69, 21.21, 14.30.



Compound **16b** – isolated primary alcohol

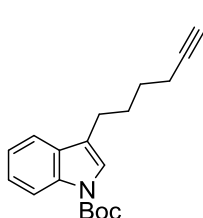
Compound **16** (4.8 g, 15.1 mmol) was dissolved in 20 mL anhydrous THF and the solution was cooled to -78°C. To this

solution, 1M DIBAL in THF (40 mL, 60.5 mmol) was added dropwise. The reaction was monitored by TLC and went to completion after 2 hours. The reaction was quenched at -78°C using a 50 mL of ETOAc and 10 mL of MeOH. This solution stirred for 1 hour and was allowed to reach room temperature. 60 mL of a pH 7 solution of citric acid was added to the quenched reaction mixture which was subsequently purified using column chromatography. Compound **16b** was isolated in 78% yield (3.4 g) in addition to starting material, compound **15** (1.0 g). ^1H NMR (400 MHz, Chloroform-*d*) δ 8.17 – 8.06 (m, 1H), 7.51 (dd, $J = 7.9, 3.7$ Hz, 1H), 7.35 (s, 1H), 7.33 – 7.27 (m, 1H), 7.22 – 7.18 (m, 1H), 2.72 (td, $J = 7.5, 3.5$ Hz, 2H), 1.84 – 1.74 (m, 3H), 1.66 (d, $J = 3.8$ Hz, 10H), 1.30 – 1.21 (m, 1H). ^{13}C NMR (101 MHz, CDCl_3) δ 130.85, 124.35, 122.50, 122.40, 121.07, 119.11, 115.39, 83.46, 77.49, 77.47, 77.36, 77.17, 77.15, 76.85, 76.83, 62.95, 32.71, 31.09, 28.41, 28.39, 25.55, 24.81, 0.15.

Compound **17**

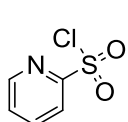
Compound **16** (3.4 g, 11.7 mmol) was dissolved in 60 mL of DCM and imidazole (2.4 g, 35.1 mmol) was stirred in at 0°C . Then, the PPh_3 (4.6 g, 17.6 mmol) was added in two equal batches separated by 15 minutes. The I_2 (4.5 g, 17.6 mmol) was dissolved in DCM and added last via cannula in two batches separated by 15 minutes as well. The reaction was stirred at 0°C for one hour then allowed to reach room temperature for an additional hour. The reaction mixture was quenched with diluted sodium bicarbonate at 0°C and the organic layer was extracted using ether. Compound **17** (4.2 g) was purified using column chromatography via a column that was packed utilizing a

solution of 5% mixture of triethyl amine and hexane for a 90% yield. ^1H NMR (400 MHz, C_6D_6) δ 8.59 – 8.46 (s, 1H), 7.45 – 7.39 (d, $J = 7.3$ Hz, 2H), 7.34 – 7.26 (t, $J = 7.7$ Hz, 1H), 7.24 – 7.20 (d, $J = 7.5$ Hz, 1H), 2.69 – 2.61 (s, 1H), 2.34 – 2.31 (s, 2H), 1.48 – 1.42 (p, $J = 3.5$ Hz, 4H), 1.41 – 1.38 (s, 9H), 0.96 – 0.89 (t, $J = 7.1$ Hz, 1H).



Compound 18

Compound 17 (4.2 g, 10.5 mmol) was dissolved in 75 mL of a 2:1 solution of ether in DMSO at 0°C . To this solution, lithium acetylide (2.0 g, 10.5 mmol) was added. The reaction mixture was allowed to stir for 1 hour at 0°C then was brought to room temperature. Reaction progress was monitored by TLC and allowed to proceed overnight. The reaction mixture was quenched at 0°C with EtOAc and sodium bicarbonate and purified using column chromatography. ^1H NMR (400 MHz, Chloroform-*d*) δ 7.91 (s, 1H), 7.60 (dd, $J = 7.9, 3.3$ Hz, 1H), 7.35 (dd, $J = 8.1, 3.6$ Hz, 1H), 7.18 (td, $J = 8.0, 7.5, 3.0$ Hz, 1H), 7.11 (ddd, $J = 10.1, 7.1, 3.3$ Hz, 1H), 6.99 (d, $J = 3.0$ Hz, 1H), 2.78 (td, $J = 7.6, 3.2$ Hz, 2H), 2.63 – 2.59 (m, 0H), 2.23 (tdd, $J = 6.9, 4.3, 2.5$ Hz, 2H), 1.55 (d, $J = 3.9$ Hz, 3H).

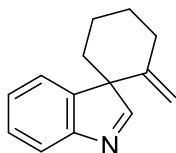


Compound 20

In a 3-neck round bottom flask, commercially available 2-mercaptopyridine (2.0 g, 17.2 mmol) was dissolved in 50 mL of concentrated sulfuric acid at 0°C . Over the course of an hour, NaClO (112 mL) was added via an addition funnel. After all of the NaClO had been added, the reaction was allowed to stir for 30 minutes at 0°C . The reaction mixture was then diluted with

30 mL of water and 30 mL of DCM and quenched with water. The aqueous layer was extracted with DCM and dried with Na₂SO₄ producing compound **20**.

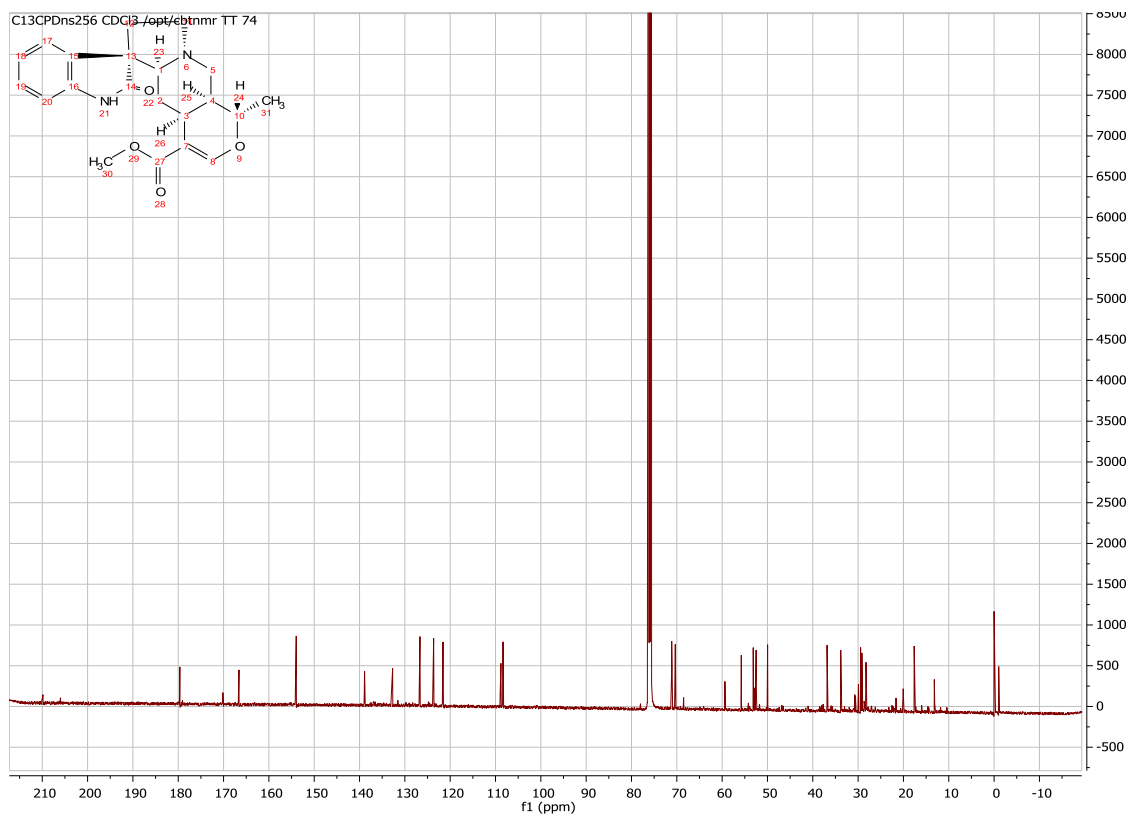
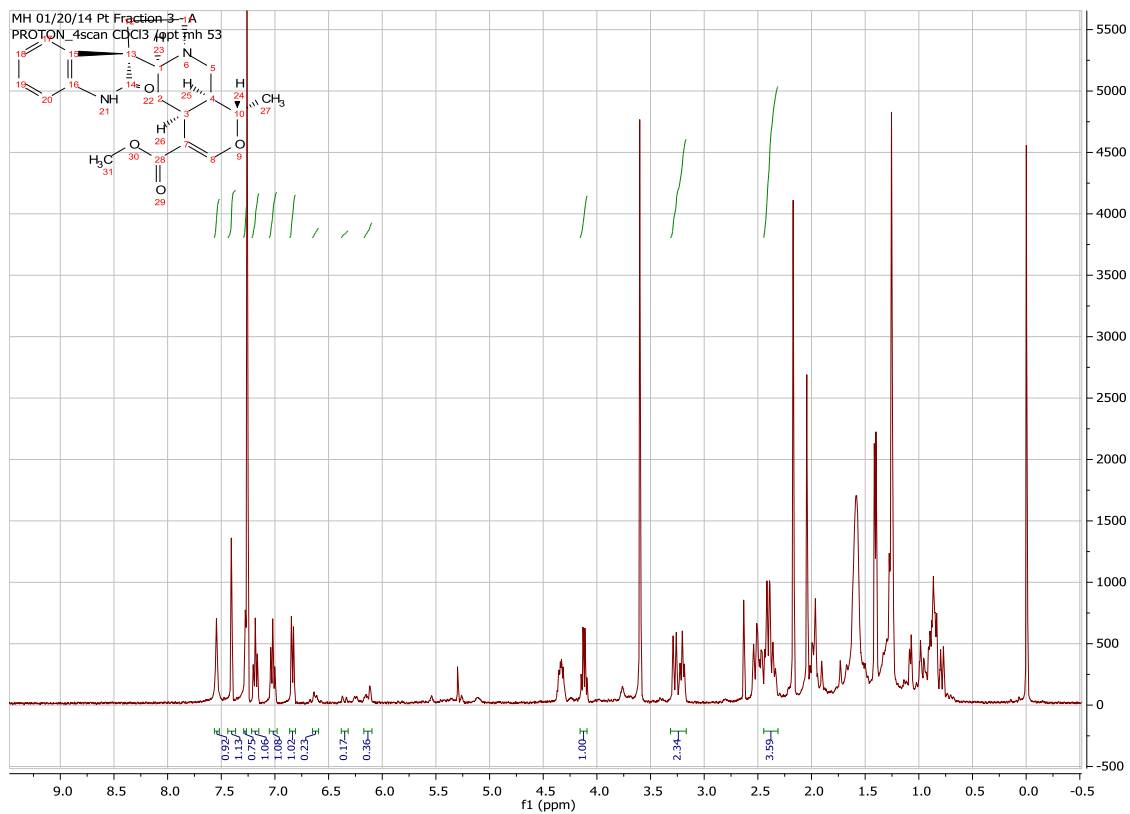
Lead Indole Cyclization Catalytic Conditions



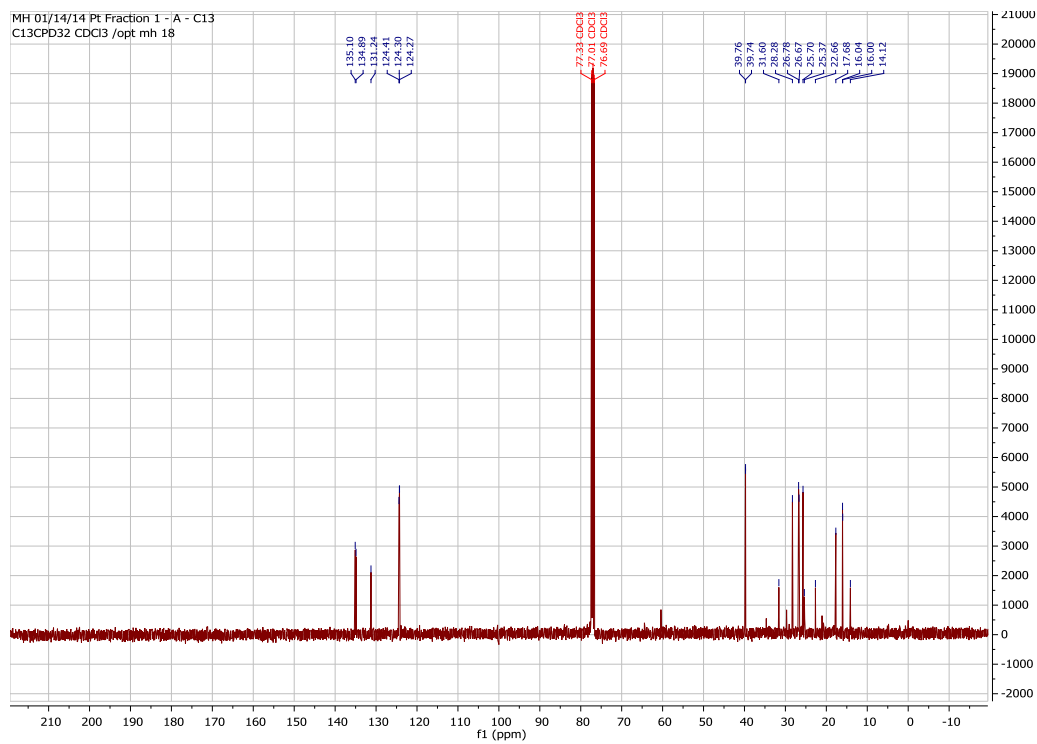
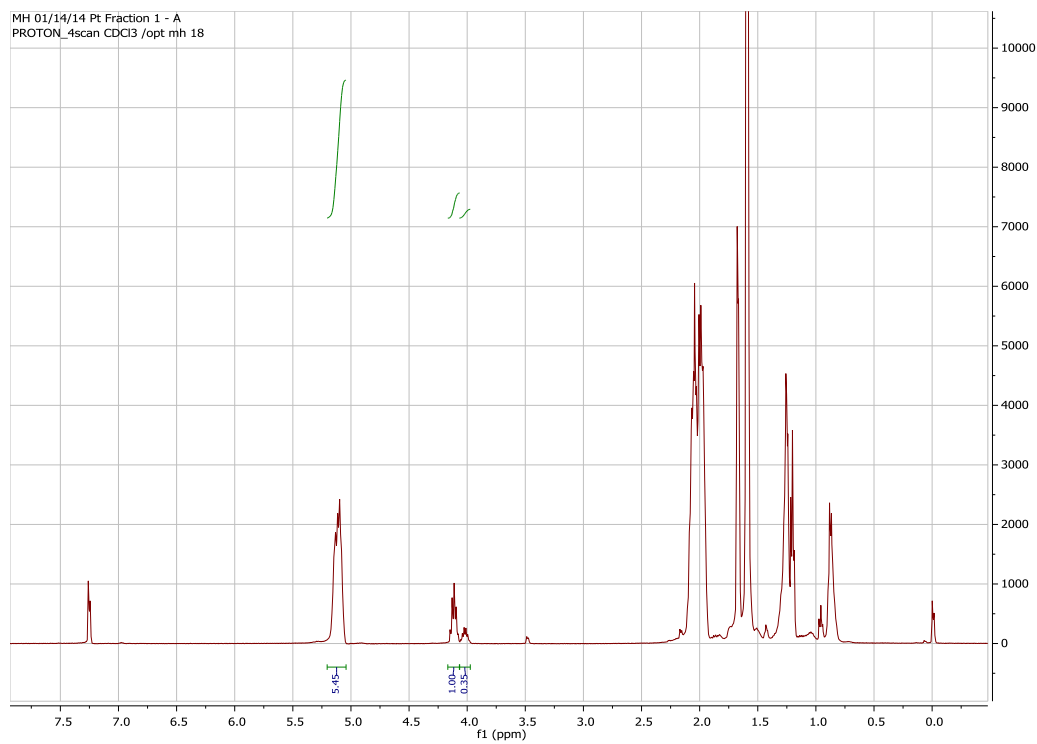
Compound **21**

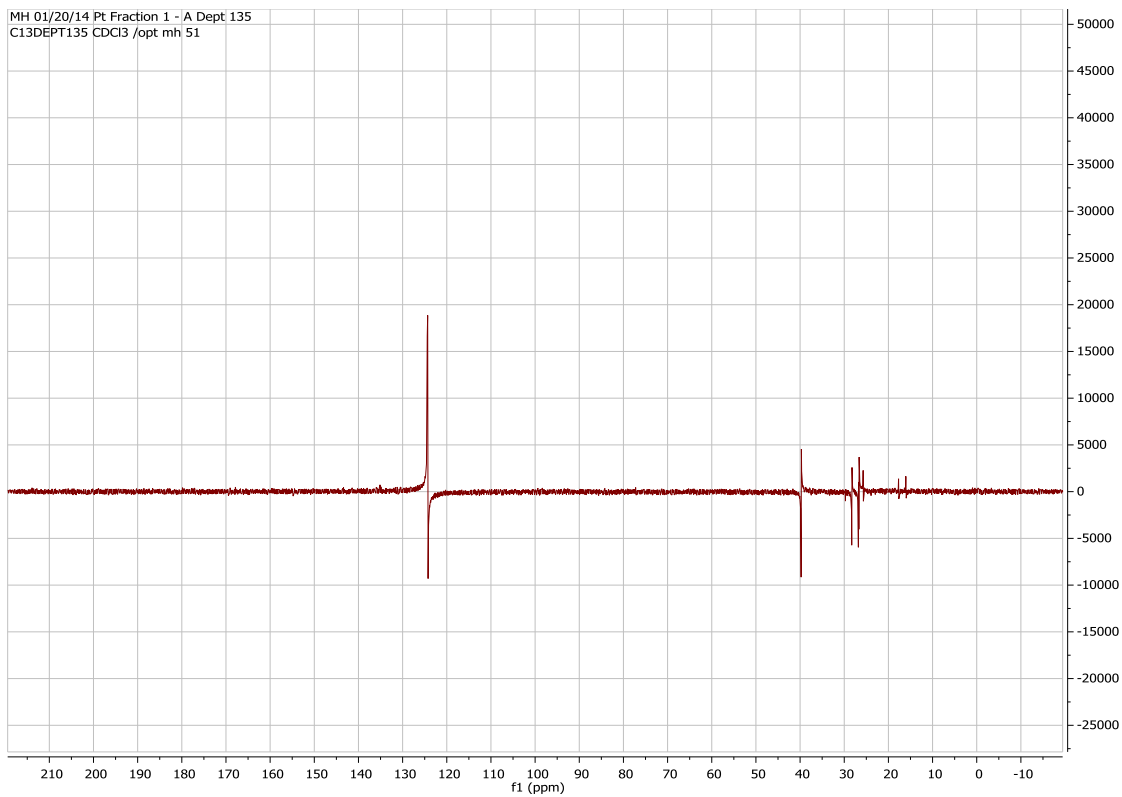
The most promising cyclized product of compound **18** utilized a combined AgOTf/In(OTf)₃ catalyst system. Compound **18** (20 mg, 0.10 mmol) was dissolved in 5 mL of DCE at room temperature and a 1:1 mixture of AgOTf (13 mg, 0.05 mmol) and In(OTf)₃ (28 mg, 0.05 mmol) was added with the ligand bi-2-naphthol (5.7 mg, 0.02 mmol). The reaction mixture was stirred for 1 hour at room temperature without the reaction proceeding. The reaction was then heated to 50°C and allowed to stir over night. The resulting reaction mixture produced the desired compound **21** in 20% yield. ¹H NMR (400 MHz, Chloroform-*d*) δ 7.79 (s, 1H), 7.47 (td, *J* = 4.7, 4.0, 2.6 Hz, 1H), 7.08 (ddt, *J* = 6.9, 4.3, 2.4 Hz, 2H), 6.95 (d, *J* = 2.8 Hz, 1H), 5.33 – 5.28 (m, 2H), 3.87 (d, *J* = 2.6 Hz, 1H), 3.08 (td, *J* = 7.2, 3.1 Hz, 1H), 2.83 (ddt, *J* = 24.3, 7.5, 3.8 Hz, 2H), 2.25 (d, *J* = 3.3 Hz, 2H), 2.10 – 1.96 (m, 0H). ¹³C NMR (101 MHz, CDCl₃) δ 150.02, 140.89, 136.25, 129.71, 128.83, 126.64, 126.34, 120.56, 118.99, 117.68, 112.74, 110.21, 77.32, 77.21, 77.01, 76.69, 53.42, 35.34, 34.32, 33.79, 32.10, 31.59, 29.97, 29.71, 28.62, 28.46, 24.38, 22.66, 20.86, 19.23, 14.13, 0.00.

Pteropodine (1)

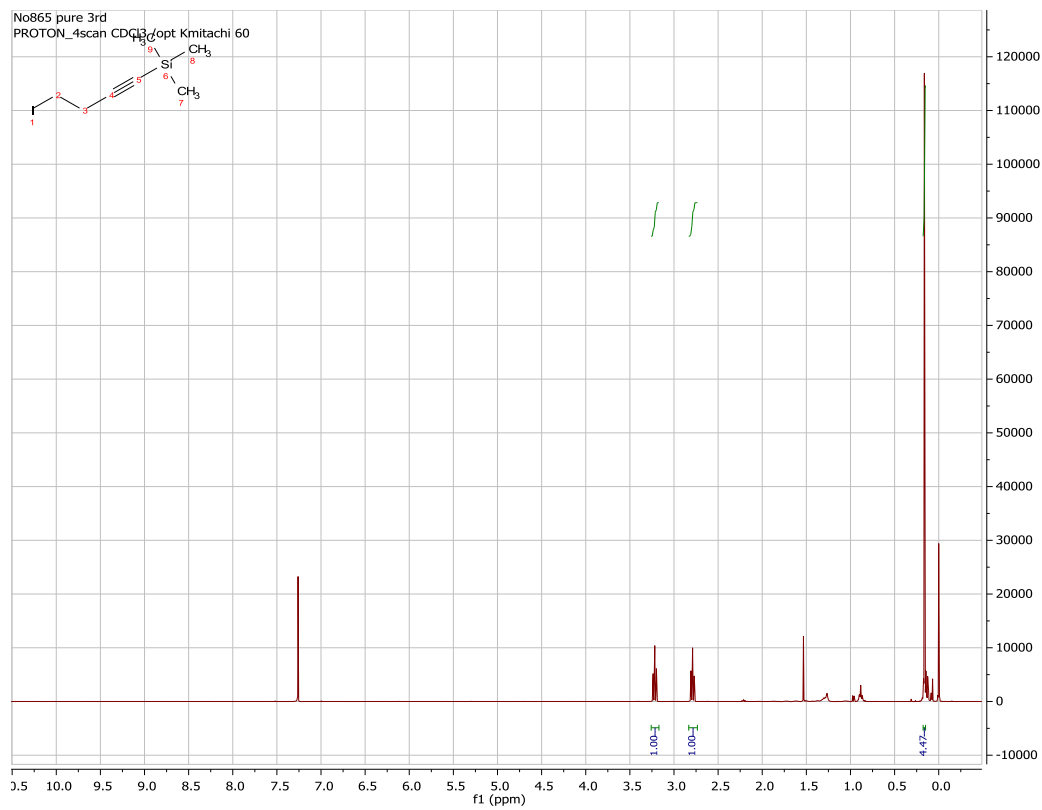


Isolated Compound (1a)

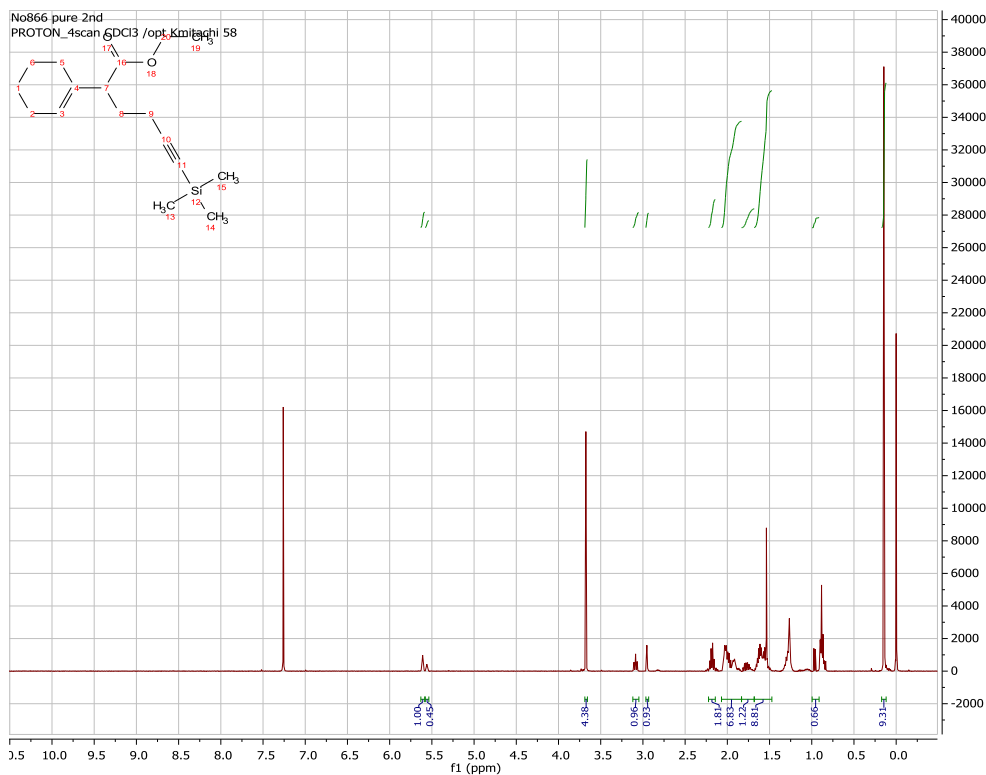




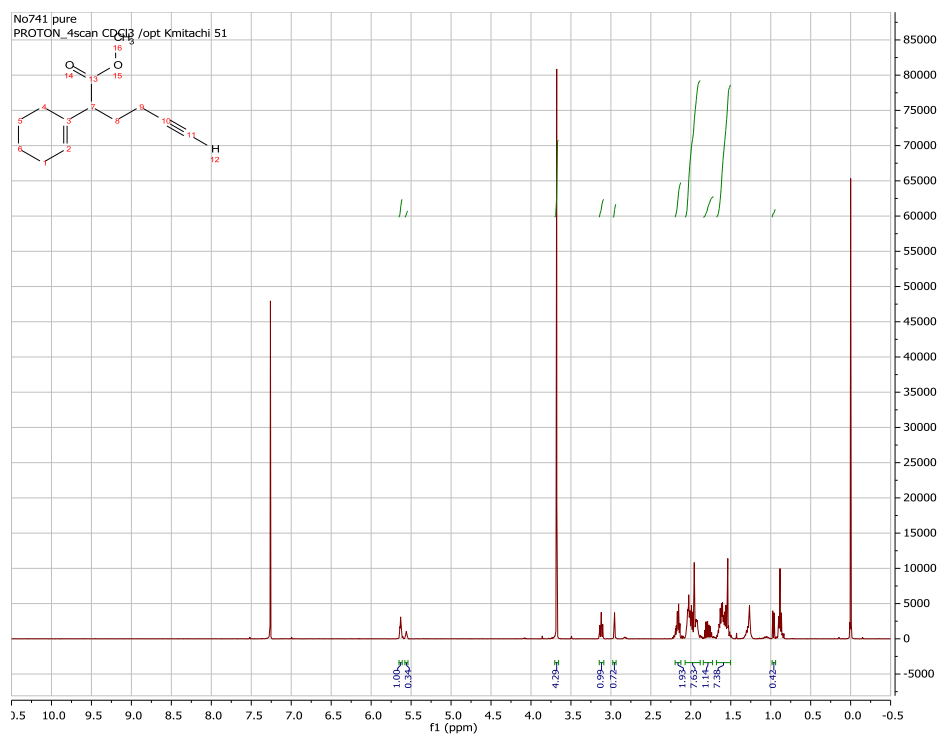
Compound 6



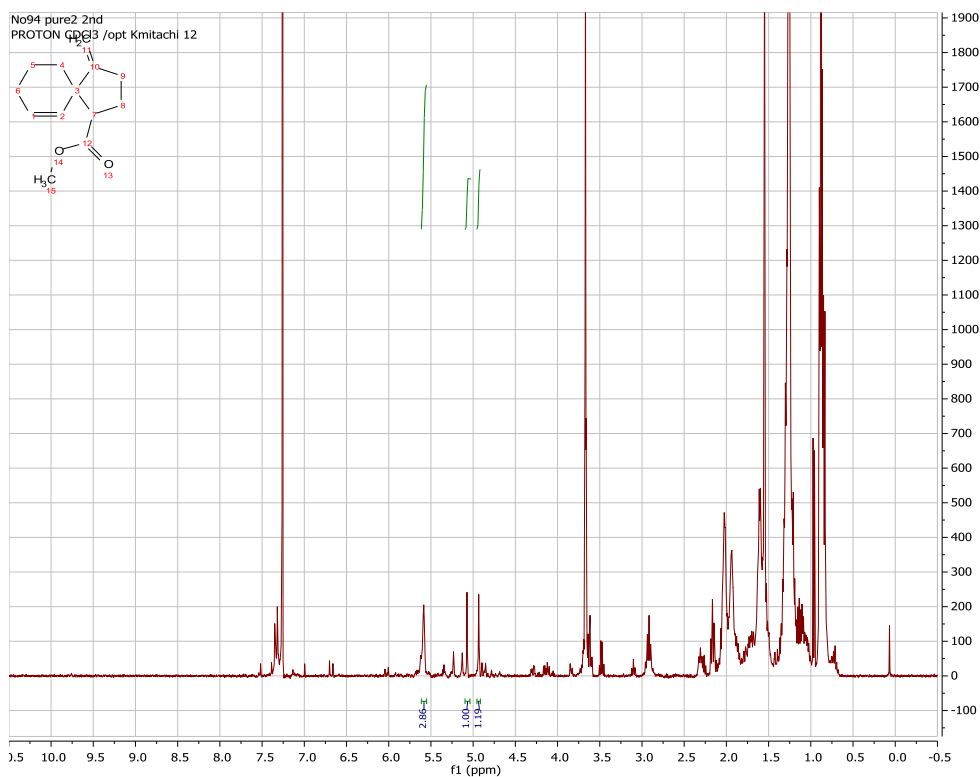
Compound 8



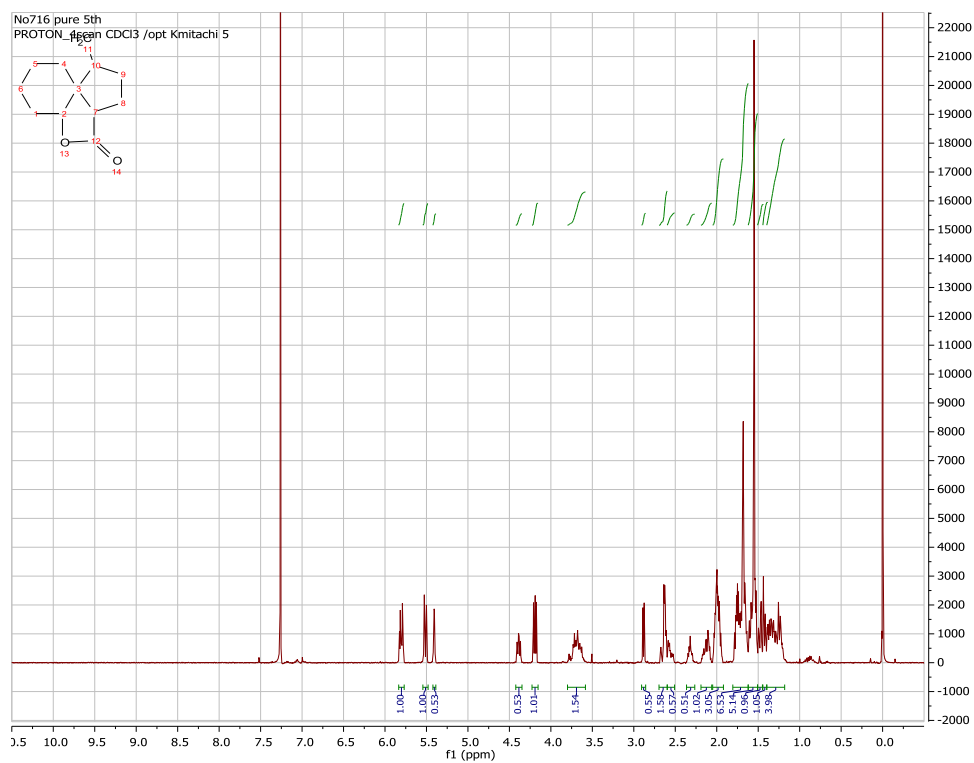
Compound 9

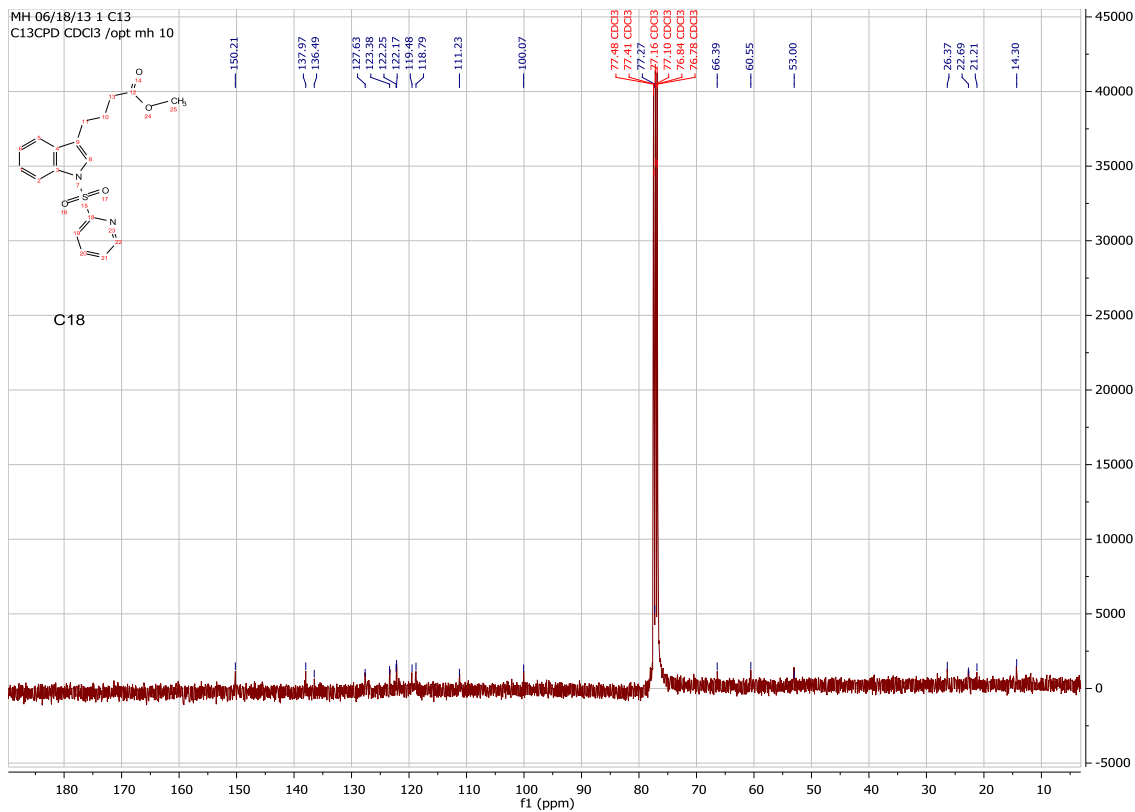


Compound 10

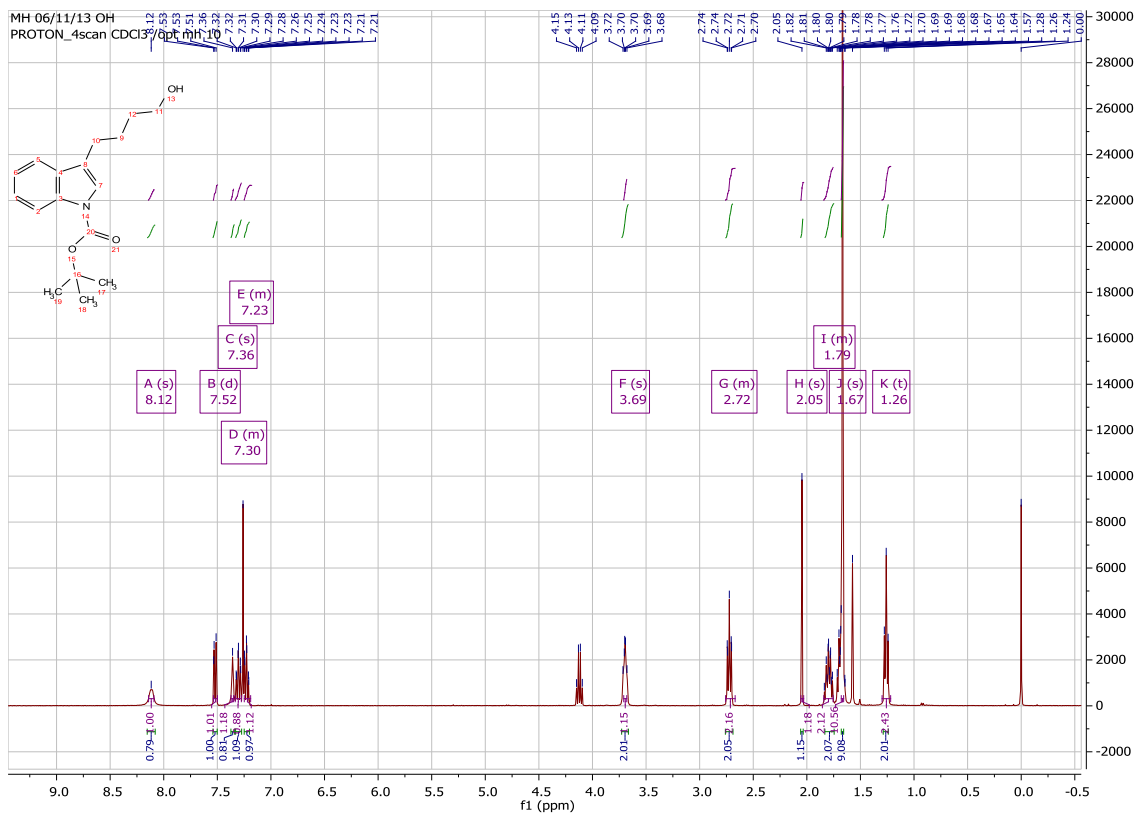


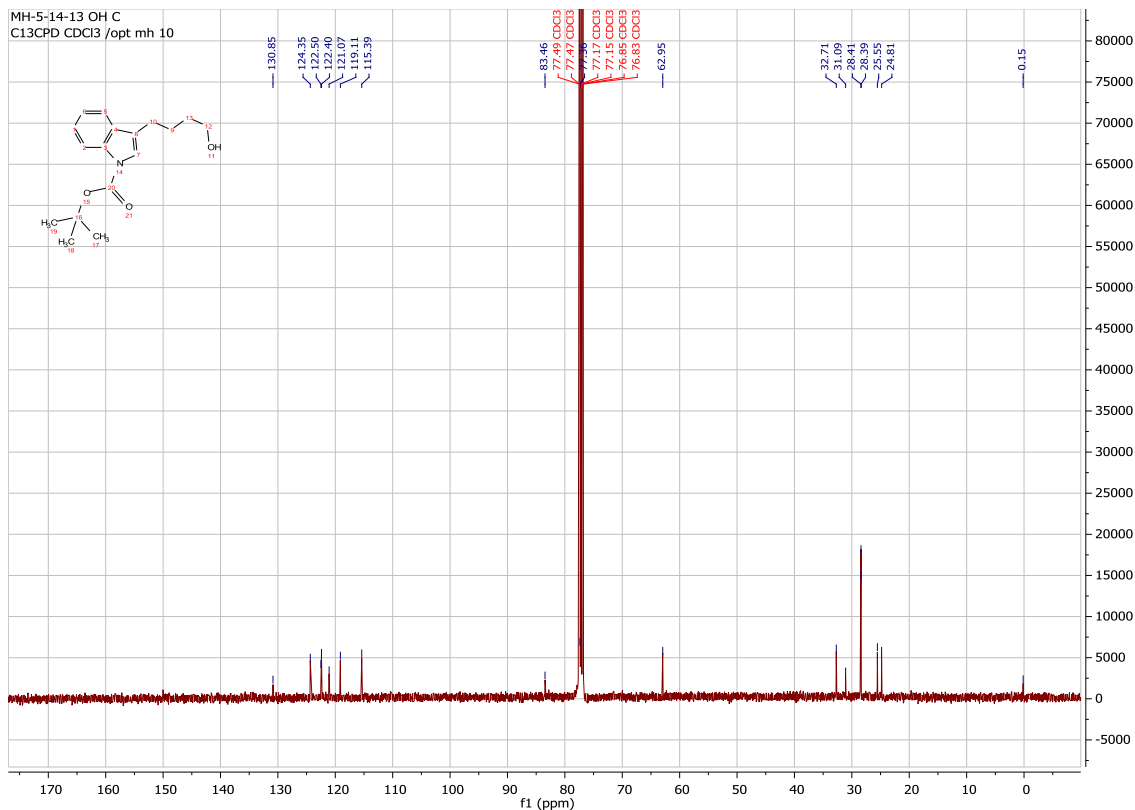
Compound 11



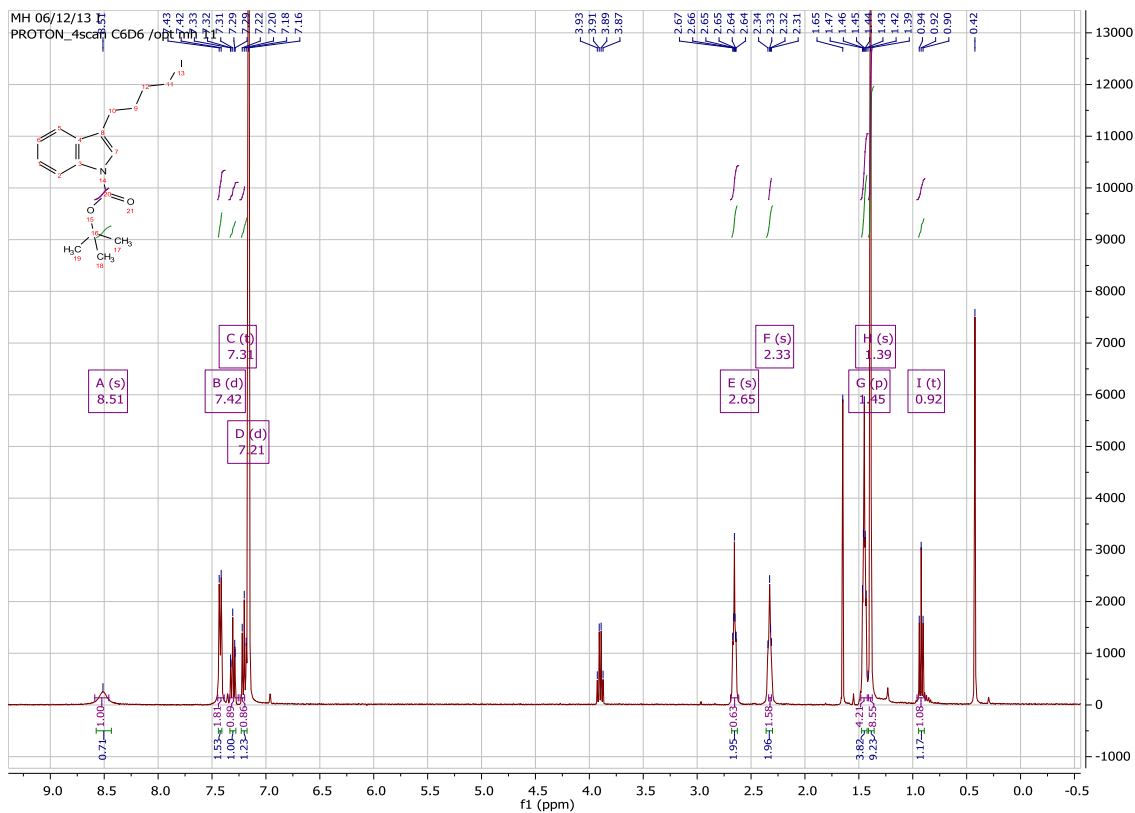


Compound 16b – isolated primary alcohol

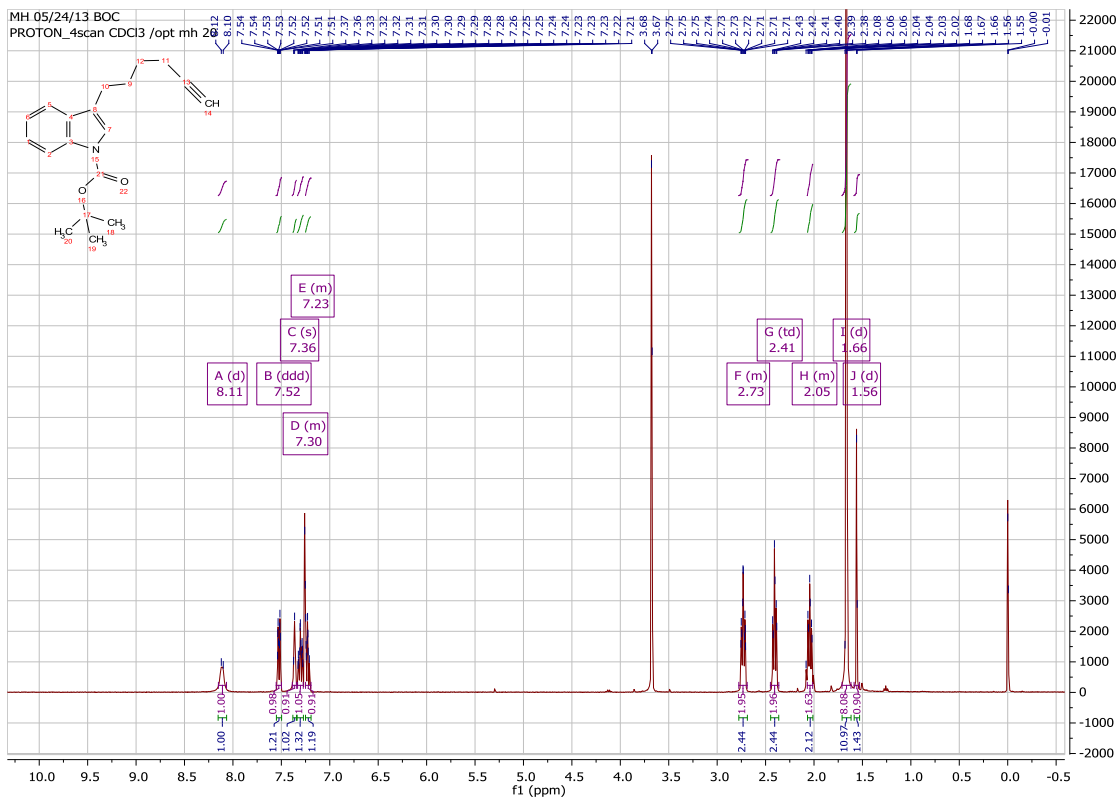




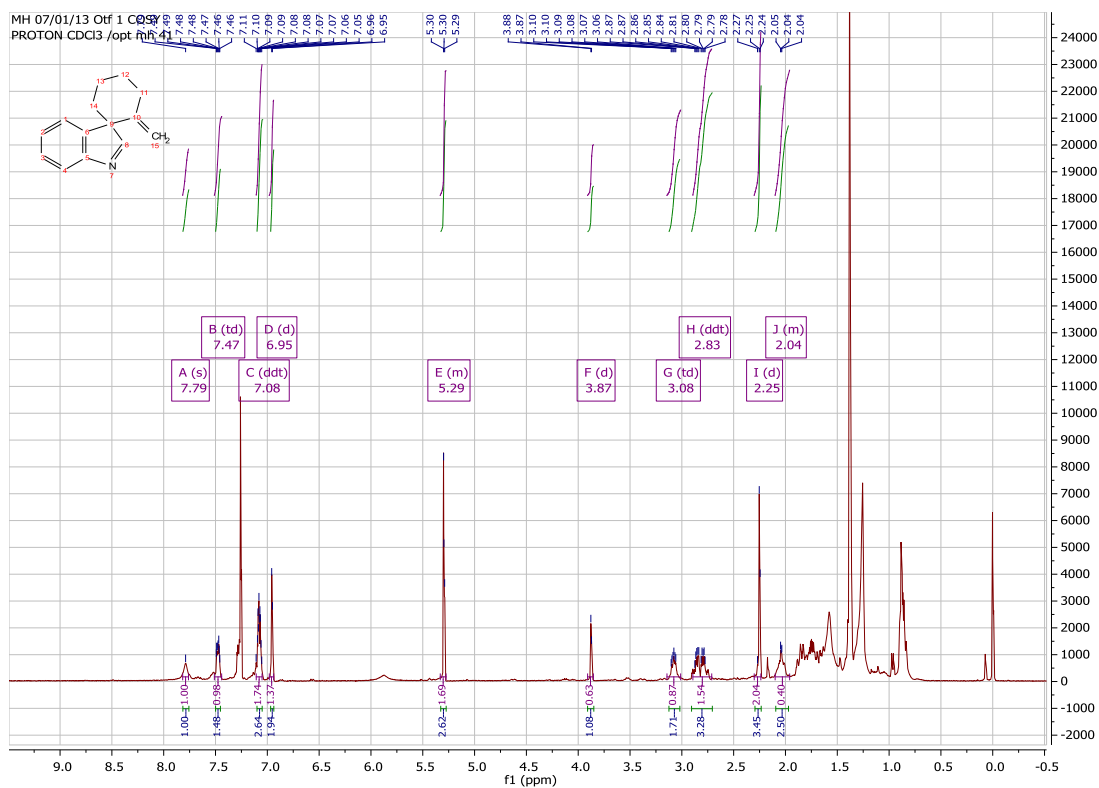
Compound 17

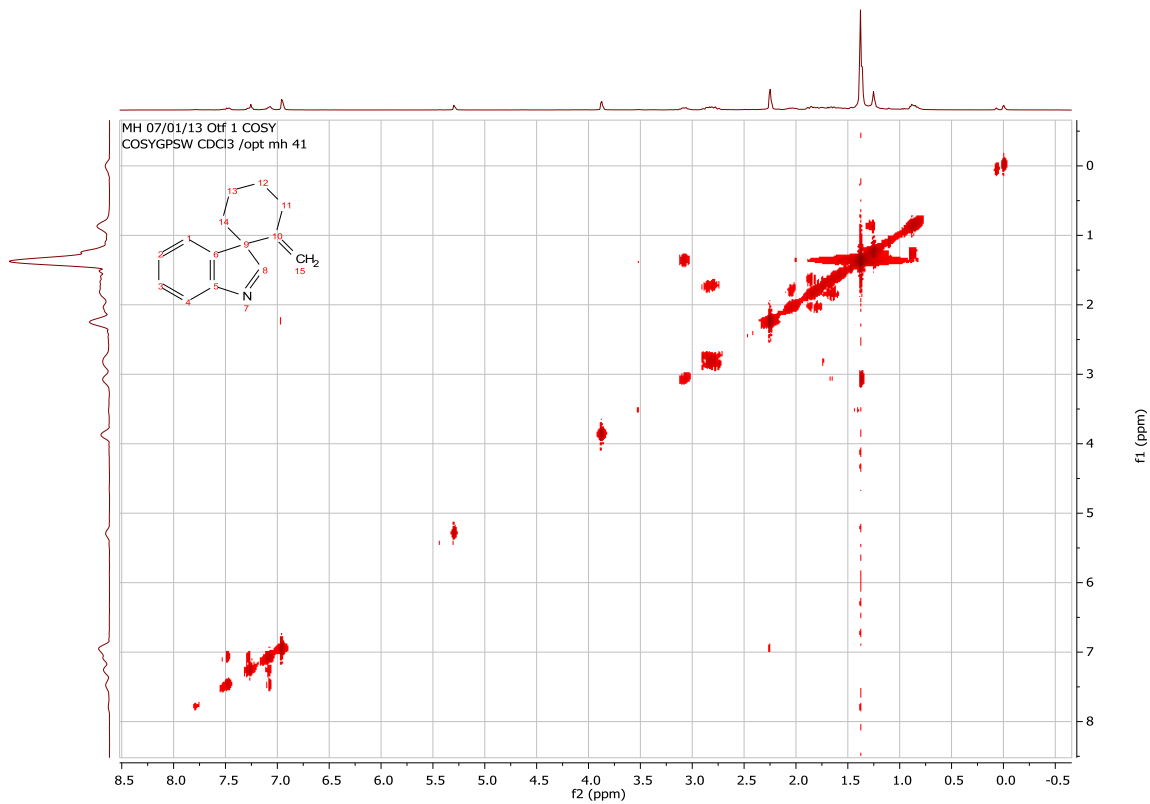
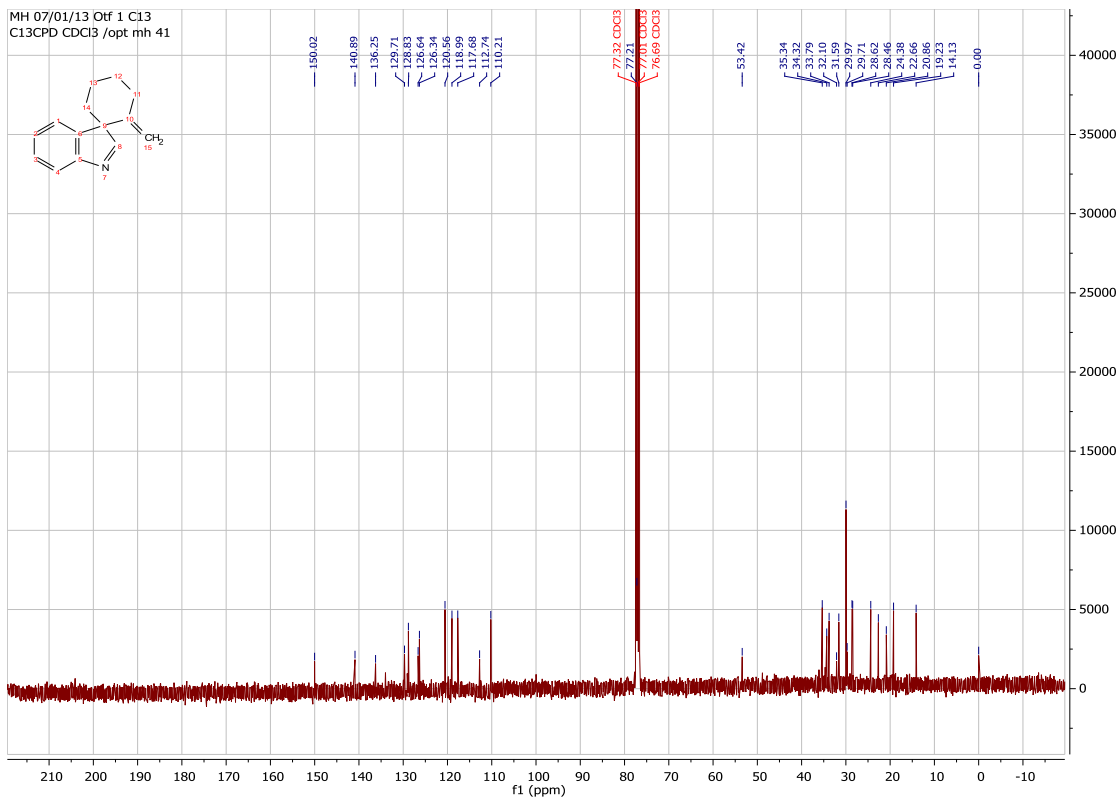


Compound 18



Compound 21





References

- [1] Cragg, G.M.; Newman, D.J.; Snader, K.M. *J. Nat. Prod.* **1997**, 60, 52-60.
- [2] Tu Y.; Jeffries C.; Ruan H.; Nelson C.; Smithson D.; Shelat A. A.; Brown K. M.; Li X.; Hester J. P.; Smillie T.; Khan I. A.; Walker L.; Guy K.; Yan B. *J. Nat. Prod.* **2010**, 73, 751–754.
- [3] Paniagua-Pérez, R.; Madrigal-Bujaidar, E.; Molina-Jasso, D.; Reyes-Cadena, S.; Álvarez-González, I.; Sánchez-Chapul, L.; Pérez-Gallaga, J. *Basic and Clinical Pharmacology and Toxicology.* **2009**, 104, 222-227.
- [4] Pilarski, R.; Filip, B.; Wietrzyk, J.; Kura, M.; Gulewicz, K. *Photomedicine.* **2010**, 17, 1133-1139.
- [5] Keplinger, K.; Laus, G.; Wurm, M.; Dierich, M.P.; Teppner, H. *J of Ethnopharmacology*, **1999**, 64, 23-34.
- [6] Kang, T.H.; Matsumoto, K.; Tohda, M.; Murakami, Y.; Takayama, H.; Kitajima, M.; Aimi, N.; Watanabe, H. *Eur. J. Pharm.*, **2002**, 444, 39-45.
- [7] Arrata. "Intramolecular ene reactions of functionalized nitroso compounds." College of London. **2010**. 26-30.
- [8] Li, J.J. "Alder ene reaction." *Name Reactions: A Collection of Detailed Reaction Mechanisms*. 2nd ed. Springer. **2003**.
- [9] Kende, A.S.; Roth, B.; Sanfilippo, P.J. *J. Am. Chem. Soc.*, **1982**, 10, 1784-1785.
- [10] Kende, A.S.; Roth, B.; Sanfilippo, P.J.; Blacklock, T.J. *J. Am. Chem. Soc.*, **1982**, 104, 5808-5810.
- [11] Aikawa, K.; Akutagawa, S.; Mikami, K. *J. Am. Chem. Soc.*, **2006**, 128, 12648-12649.
- [12] Lazarus, G.S.; Cooper, D.M.; Knighton, D.R.; Margolis, D.J.; Percoraro, R.E.; Rodeheaver, G.; Robson, M.C. *Wound Repair and Regeneration.* **1994**, 2, 165-170.
- [13] Guo, S.; DiPietro, L.A.; *J. Dent. Res.*, **2010**, 89, 291-229.
- [14] Eftekhari, A. "Accelerating Wound Closure in Patients with Diabetetes." *Am. Diabetes Association.* **2012**.
- [15] Berlanga-Acosta, J.; Gavilondo-Cowley, J.; Barco-Herrera, D.G.; Martin-Machado, J.; Guillen-Nieto, G. *J Carcinogenesis and Mutagenesis.* **2011**, 2:1.
- [16] Waugh, H.V.; Sherratt, J.A. *Bulletin of Mathematical Biology*, **2006**, 68, 197-207.
- [17] "Wound Healing Assay: Gap Closure Migration Assays." Cell Biolabs, Inc. **2013**.
- [18] Gauger, K.S.; Rodriguez-Cortes, A.; Hartwich, M.; Schneider, S.S. *J. Med. Plants Research.* **2010**, 4, 446-454.
- [19] Newman, D.J.; Cragg, G.M. *J. Nat. Prod.* **2012**. 75, 311-335.
- [20] Garcia-Rubia, A.; Urones, B.; Arrayas, R.G.; Carretero, J.C. *Chem. Eur. J.*, **2010**, 16, 9676-9685.
- [21] Green, T.W.; Wuts. P.G.M. "Protection for imidazoles, pyrroles, indoles, and other aromatic heterocycles." *Protective Groups in Organic Synthesis*. 3rd ed. John Wiley & Sons. **1999**. 615-631